Journal Pre-proof

Hydrothermal synthesis of $BiOX/Bi_2WO_6/Bi_2S_3$ ternary heterostructures for enhanced solar light photocatalytic degradation of ciprofloxacin in aquatic media

Muhammad Naeem, Muhammad Imran, Shoomaila Latif, Adnan Ashraf, Mohammad Mahbubul Hassan, Muhammad Naeem Khan

PII: S0920-5861(26)00017-9

DOI: https://doi.org/10.1016/j.cattod.2026.115693

Reference: CATTOD115693

To appear in: *Catalysis Today*

Received date: 19 September 2025
Revised date: 16 January 2026
Accepted date: 19 January 2026

Please cite this article as: Muhammad Naeem, Muhammad Imran, Shoomaila Latif, Adnan Ashraf, Mohammad Mahbubul Hassan and Muhammad Naeem Khan, Hydrothermal synthesis of $BiOX/Bi_2WO_6/Bi_2S_3$ ternary heterostructures for enhanced solar light photocatalytic degradation of ciprofloxacin in aquatic media, *Catalysis Today,* (2026) doi:https://doi.org/10.1016/j.cattod.2026.115693

Hydrothermal synthesis of $BiOX/Bi_2WO_6/Bi_2S_3$ ternary heterostructures for enhanced solar light photocatalytic degradation of ciprofloxacin in aquatic media

Muhammad Naeem[1], Muhammad Imran[1*], Shoomaila Latif[1], Adnan Ashraf[2], Mohammad Mahbubul Hassan[3*], Muhammad Naeem Khan[1]

[1] Center for Inorganic Chemistry, School of Chemistry, University of the Punjab, Quaid-e-Azam Campus, Lahore, 54590, Pakistan.

[2]Department of Chemistry, The University of Lahore, Pakistan.

[3]Fashion, Textiles, and Technology Institute, University of the Arts London, 105 Carpenter's Road, London E20 2AR, United Kingdom.

Abstract

The presence of trace levels of antibiotics in drinking water poses a serious concern as it contributes to the development of antibiotic resistance in bacteria. In this study, various bismuth-based ternary heterostructure photocatalysts were synthesized by combining $BiOX/Bi_2WO_6$ (where X = Cl, Br, or I) heterostructures with Bi_2S_3 at a molar ratio of 1:1:1. The X-ray deffraction (XRD) and scanning electron microscopy (SEM) analyses confirmed the successful synthesis of $BiOX/Bi_2WO_6/Bi_2S_3$ ternary heterostructures with tunable band gaps, while the

* Corresponding authors:
Email: imran.hons@pu.edu.pk (M. Imran)
mahbubul.hassan@arts.ac.uk (M. M. Hassan)

photoluminescence (PL) spectroscopy indicated enhanced charge separation. The photocatalytic performance of these ternary heterostructures was evaluated by degrading ciprofloxacin (CFX) in an aqueous solution under solar light. All the ternary heterostructures, namely $BiOCl/Bi_2S_3/Bi_2WO_6$ (BWS-Cl), $BiOBr/Bi_2S_3/Bi_2WO_6$ (BWS-Br), and $BiOI/Bi_2S_3/Bi_2WO_6$ (BWS-I), demonstrated excellent photodegradation of CFX within 120 min. The degradation rate constant (k) for CFX using the BWS-Cl heterostructure was 0.023 min^{-1}. The effect of catalyst dosage, CFX concentration, and the initial pH of the drug solution on the photocatalytic degradation performance of CFX was also examined. Notably, the BWS-Cl exhibited the highest degradation efficiency at 96.6%, achieved under sunlight with an optimized catalyst dosage of 0.6 g/L and an initial ciprofloxacin concentration of 5 ppm at a pH of 9.00. Based on the results from radical trapping experiments and PL analysis, a potential degradation mechanism for CFX by these heterostructures was proposed. The stable and reusable ternary heterostructure photocatalysts developed in this work may find applications in the removal of CFX and other similar emerging organic pollutants from potable water.

Keywords: Ternary heterostructures; Bismuth-based photocatalysts; Ciprofloxacin degradation; Solar-light photocatalysis; Reuseable

1. Introduction

Drinking water pollution with medicinal wastes, especially antibiotics, is a serious concern due to potential risks to human health and the environment. Antibiotic contamination can lead to the development of antibiotic-resistant bacteria, making infections harder to treat [1]. Furthermore, even low levels of antibiotics in drinking water can have negative impacts on aquatic ecosystems [2]. The long-term consumption of antibiotic-contaminated water primarily leads to the development of superbugs, making infections in humans difficult or impossible to treat, and also risks of direct toxic effects on human organs and disruption of the body's natural microbiome, as suggested by a recent study [3].

In various pharmaceutical waste degradation studies, ciprofloxacin (CFX) is used as a model antibiotic because its photocatalytic degradation can easily be monitored by UV-vis spectroscopy. CFX belongs to the third generation of fluoroquinolone antibiotics, which is more commonly used than other antibiotics because of its excellent activity against Gram-negative bacteria, especially against *Staphylococcus sp.* [4]. However, CFX is not fully metabolized in the human body, and the unmetabolized drug is excreted through urine and feces [5]. CFX enters surface water primarily through human and animal waste and agricultural runoff. The currently used wastewater treatment plants often cannot remove it fully, leading to its release into the environment. Additionally, improper disposal of unused medications and agricultural practices involving animal waste also contribute to its presence in surface water [6]. The presence of residual CFX in the environment may lead to the emergence of antibiotic-resistant bacteria and an increase in the concentration of CFX in the food chain, endangering human and animal health.

Hence, the efficient degradation of antibiotic pollutants in potable water has emerged as a subject of continuing study for developing efficient water treatment techniques. [7–9].

Of the various techniques developed over the years for the removal of pharmaceutical waste, especially antibiotics, from potable water. Of them, photocatalytic degradation has been considered as a viable technology and green technology for the degradation of highly hazardous and toxic pollutants because of its appreciable low operating cost without the production of any secondary products [10]. In this method, solar energy is converted into chemical energy with very high degradation efficiency through the generation of active species, such as hydroxyl and superoxide radicals [11,12]. The photocatalysts developed over the years can be categorized into solar visible light and UV radiation-activated photocatalysts. The UV-activated photocatalysts have many demerits, including the requirement for UV light, which only uses a small part of the solar spectrum, leading to limited energy efficiency, and they can also cause undesirable side reactions. Conversely, visible-light photocatalysts offer a significant advantage over UV-activated photocatalysts because they can utilize a broader spectrum of sunlight. They can work even when the sky is cloudy, making them very efficient, sustainable, and practical for various applications [13].

Recently, various heterostructure visible-light photocatalysts, such as $Mn_2O_3/Mn_3O_4/MnO_2$ [14], metal/g-C_3N_4/ZnO [15], $CuFe_2O_4/ZnIn_2S_4$ [16], Cu–ZnO/S-gC_3N_4 [17], and S-gC_3N_4@ Co-Zn_xFe_3-xO_4 [18], have been developed. They offer several advantages over traditional photocatalysts used in various applications, including enhanced light absorption, improved charge separation and transfer, and better control over band alignment, leading to increased photocatalytic efficiency. Metal sulfides have also drawn interest due to their narrow band gaps, allowing them to absorb visible light, unlike wider-bandgap metal oxides, and their S 3p-

dominated valence bands offer superior charge separation for applications like solar energy conversion, water splitting, and CO_2 reduction [19,20]. Having a low direct band gap, high absorption coefficient, and high incident photon-to-electron conversion efficiency, Bi_2S_3 is one of the most-studied metal sulfides. The main drawbacks for its photocatalytic applications may include its poor stability, high charge carrier recombination rates, and photo corrosion [21,22]. Previous research suggests that its photocatalytic performance can be enhanced by forming heterostructures with other suitable semiconductors, such as Bi_2WO_6, Cu_2S, $CoWO_4$, CeO_2, $BiVO_4$, and BiOCl [23–25]. S-scheme heterojunctions have also attracted considerable attention in photocatalysis due to their reported ability to effectively separate photogenerated charge carriers, which helps retain strong redox potential. This mechanism is considered highly beneficial for improving the efficiency of photocatalytic reactions compared to traditional Z-scheme or Type-II heterojunctions [26,27].

Another class of semiconductors for photocatalytic applications is the tungsten-based materials, such as $CoWO_4$, $CuWO_4$, $ZnWO_4$, WO_3, and Bi_2WO_6, which have been extensively investigated due to their high photo-oxidation performance. Bismuth-based ternary heterostructure photocatalysts, such as $Ag/Bi_2MoO_6/ZnO$ [4], and $Bi_2S_3/BiWO_6/rGO$ [28], are reported to be highly efficient visible-light photocatalysts. BiOX (Cl, Br, I) compounds are widely used in photocatalytic applications, particularly in environmental remediation, such as the degradation of organic pollutants in wastewater. Their unique lamellar structure promotes the efficient separation of photogenerated electron-hole pairs, a critical factor in photocatalytic activity. The primary drawbacks of BIOX are their limited visible light utilization efficiency (for BiOCl), rapid recombination of photogenerated charge carriers, and stability issues in certain conditions [29]. To improve the photocatalytic efficiency of BIOX compounds, various efforts

have been made, such as the formation of heterojunctions, elemental doping, defect engineering, and thickness tuning [30].

Bismuth-based heterostructure photocatalysts are known for their ability to efficiently utilize sunlight, narrow band gaps, and strong charge separation, leading to enhanced photocatalytic activity [31]. These materials have a large surface area and have excellent characteristics such as low time for the detachment of charges and high electronic conductivity [32]. Currently, ternary composites have received much attention for the photocatalytic removal of organic pollutants from wastewater. For example, published research shows that NH_2-UiO-66/BiOBr/Bi_2S_3 [33], CdS/MoS_2/Bi_2S_3 [34] and Ag_2S/AgI-Bi_2S_3/BiOI [35] effectively degraded tetracycline (TC), methylene blue (MB), and salicylic acid (SA), and the photodegradation efficiency reached 95.23, 90.0 and 89.2% within 400, 120 and 360 min respectively [35]. All bismuth-based few ternary heterostructure photocatalysts with enhanced photocatalytic performance, such as α-Bi_2O_3/β-Bi_2O_3/Bi_5O_7 [36], BiOCl/$(BiO)_2CO_3$/Bi_2O_3 [37], BiOCl/$Bi_{12}O_{17}Cl_2$/Bi_2O_3 [38] and BiOI/$Bi_4O_5I_2$/$Bi_2O_2CO_3$ [39] have also been reported and their photocatalytic degradation of Bisphenol A, mixture of methyl orange and phenol, CFX, and TC hydrochloride reached 80.4, 67, 95.2, and 80.2% respectively. The photocatalytic degradation of CFX by BiOCl/$Bi_{12}O_{17}Cl_2$/Bi_2O_3 was reported to be more than 85% [38]. Therefore, highly stable and low-cost all bismuth-based ternary heterostructures, such as BiOX/Bi_2WO_6/Bi_2S_3, are expected to provide high photocatalytic activity.

This study reports the synthesis of novel all-bismuth ternary heterostructures, BiOX/Bi_2WO_6/Bi_2S_3 (X = Cl, Br, or I) by a two-step hydrothermal/calcination process and its application for the photocatalytic degradation of ciprofloxacin. The literature review reveals that they were never studied for the visible-light photocatalytic degradation of ciprofloxacin. In this

work, we used halogen ions (Cl, Br, and I) doping into the bismuth oxide structural framework and measured the effect of charge separation and band alignment. The optimized BWS-Cl has a significantly higher degradation efficiency and rate constant than the reported Bi-based photocatalysts, which is indicative of its high redox capacity and effective electron-hole separation. Bismuth compounds, which are widespread on Earth, are not toxic and are produced at a low temperature, highlighting the pragmatic benefits of this heterostructure in scalable solar-driven water treatment.

2. Experimental section

2.1. Materials

Sodium tungstate dihydrate ($Na_2WO_4 \cdot 2H_2O$), potassium chloride (KCl), potassium bromide (KBr), potassium iodide (KI), nitric acid (HNO_3), and sodium hydroxide (NaOH) were purchased from Sigma Aldrich. Bismuth nitrate pentahydrate ($Bi(NO_3)_3.5H_2O$) was bought from Unichem (China). Thiourea and CFX hydrochloride were procured from Spectrum Chemicals (Pakistan) and Kabeer Pharmacare Pvt. Ltd. (Pakistan), respectively. Absolute ethyl alcohol was purchased from Merck. All chemicals used in this work were of analytical reagent grade and were used without any further purification.

2.2. Synthesis of photocatalysts

2.2.1. Synthesis of binary BiOX/Bi_2WO_6 heterojunction

The $BiOX/Bi_2WO_6$ (X = Cl, Br, I) binary composites were synthesized by the hydrothermal method as reported by others [40]. In brief, 10 mmol $Bi(NO_3)_3 \cdot 5H_2O$ was dissolved in 30 mL of distilled water and ultrasonicated for a few minutes, and then magnetically stirred. A clear solution of precursor was obtained by dropwise addition of 3M nitric acid. A 2.5 mmol $Na_2WO_4 \cdot 2H_2O$ solution was prepared, and a 5 mmol potassium halide (KCl, KBr, KI) solution was added to it. The mixture of Na_2WO_4/KX solution was then transferred to a 100 mL Teflon-lined stainless-steel autoclave and heated at 160 °C in an oven for 14 h. After the hydrothermal treatment, the cylinder was cooled, and the precipitates were filtered using Whatman filter papers. They were then washed repeatedly with distilled water and lastly with ethyl alcohol. The synthesized $BiOX/Bi_2WO_6$ was dried in an oven at 85 °C for 12h.

2.2.2. Synthesis of Bi_2S_3

3 mmol of $Bi(NO_3)_3.5H_2O$ was dissolved in 40 mL of deionized water and stirred for 30 min. A few drops of 3M nitric acid were added to it to get a clear solution. 6 mmol of thiourea solution was added to the above solution and stirred again for 60 min. The precursor solution of bismuth nitrate and thiourea was transferred to a 100 mL Teflon-lined stainless-steel autoclave and heated in a hot air oven at 160 °C for 16 hours. After cooling the system at room temperature, the precipitates were filtered and washed with deionized water and finally with ethanol. The washed material was dried at 80 °C for 8 h.

2.2.3. Synthesis of $BiOX/Bi_2WO_6/Bi_2S_3$ heterostructures

The heterostructure photocatalysts $BiOX/Bi_2WO_6/Bi_2S_3$ were prepared by calcination. The binary composites $BiOX/Bi_2WO_6$ and Bi_2S_3 at an equal mol ratio were dissolved in 30 mL of

ethyl alcohol and then sonicated for 30 min. After sonication, the mixture was stirred continuously with slow heating to evaporate the solvent. The finally obtained heterostructure photocatalysts were heated at 100 ℃ for 2 h, followed by grinding to achieve a fine powder. The obtained BiOX/Bi_2WO_6/Bi_2S_3 heterostructure photocatalyst powder was calcined at 350 °C for 4 h. The synthesis process of BiOX/Bi_2WO_6/Bi_2S_3 is shown by a schematic diagram in Fig. 1.

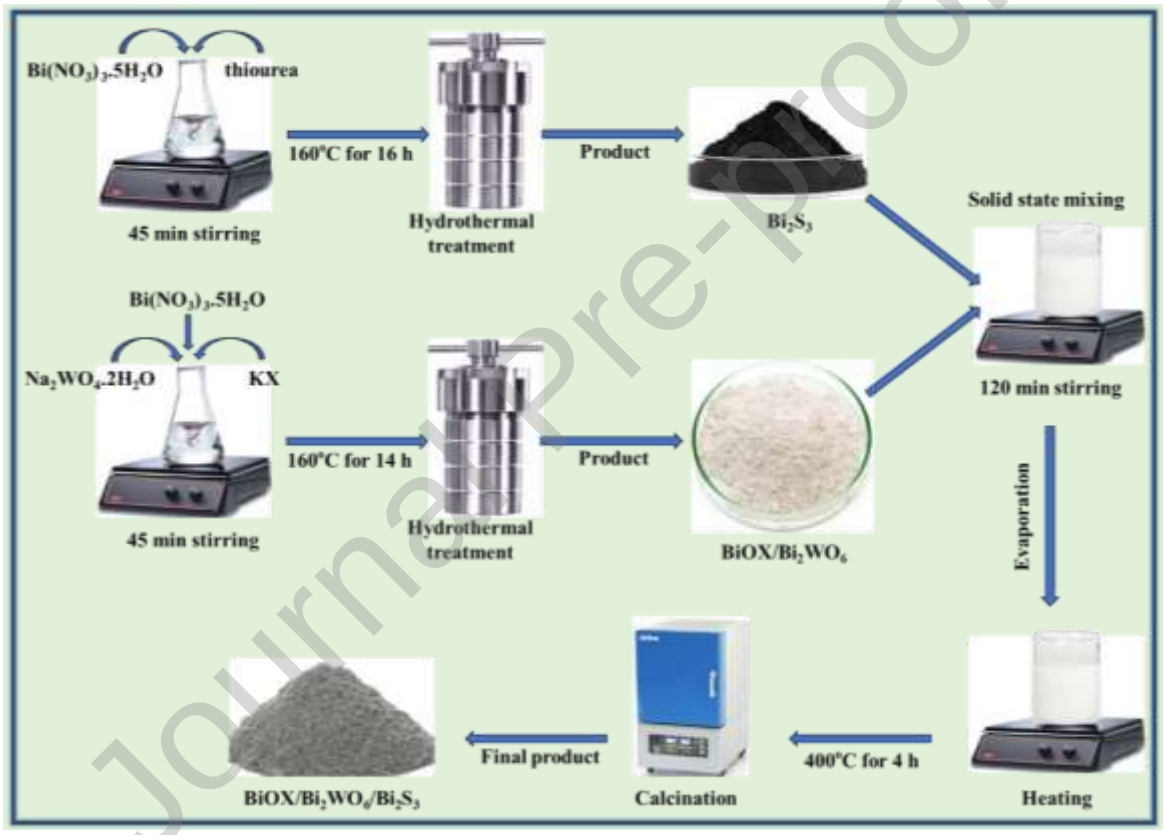

Fig. 1. Schematic diagram for the synthesis of BiOX/Bi_2WO_6/Bi_2S_3 ternary heterostructures via the hydrothermal method, followed by calcination.

2.3. Characterization of BiOX/Bi_2WO_6/Bi_2S_3 heterostructures

The characterization of optical properties and band gap was performed using a UV-visible (Model: UV-6100, Hinotek, China) and Nicolet Fourier transform infrared (FTIR) (Model: iS5, ThermoFisher Scientific Corporation, USA) spectrometers. A Bruker powder X-ray diffractometer (XRD) (Model D8, Bruker Scientific Instruments, USA) using Cu Kα radiation of 0.15456 nm wavelength was used to analyze the crystallite size and microstructural properties of the various heterostructure photocatalysts at 2θ angles from 20 to 80°. The elemental analysis of the photocatalysts was carried out by using a scanning electron microscope (SEM) (model: FEI Nova 450, Thermo Fisher Scientific, USA) equipped with an energy dispersive X-ray (EDX). The photoluminescence (PL) of the photocatalyst samples was carried out by a photoluminescence spectrometer (Model: FS-5, Edinburgh Instruments, UK) equipped with an HBO 100 W xenon arc lamp. The photocatalytic degradation of CFX was measured by the UV/Visible spectrophotometer mentioned earlier.

2.4. Photocatalytic degradation of CFX by heterojunction photocatalysts

The photocatalytic degradation of CFX by various synthesized BiOX/Bi_2WO_6/Bi_2S_3 heterostructures was carried out in a photocatalytic quartz glass reactor under sunlight. A specified amount of an aqueous solution of a certain concentration of CFX was taken in the glass reactor, and to it a certain quantity of heterostructure photocatalysts was added. The mixture was left in dark conditions for 15 min to reach the adsorption-desorption equilibrium, to measure the removal of CFX by adsorption. Then the reactor was placed under natural sunlight in July, in a daytime from 11:00 to 13:00 (weather conditions are sunny at about 47 ºC) in Lahore, Pakistan (31.5204°N, 74.3587°E), and a 4 to 5 mL amount of the sample was withdrawn from the test

solution at regular intervals of time and filtered. The degradation of the CFX was measured by using a UV-Vis spectrophotometer at λ_{max} = 270 nm. The degradation efficiency was measured by using the following formula [41]:

$$Degradation\ (\%) = \frac{C_0 - C_t}{C_0} \times 100 \qquad (1)$$

where C_0 and C_t are the concentration of the CFX at time 0 and t, respectively. Our research focused on optimizing photodegradation performance by examining four crucial degradation parameters of the synthesized heterostructure photocatalysts, which include irradiation time, pH of the reaction mixture, catalyst dosage, and initial concentration of CFX.

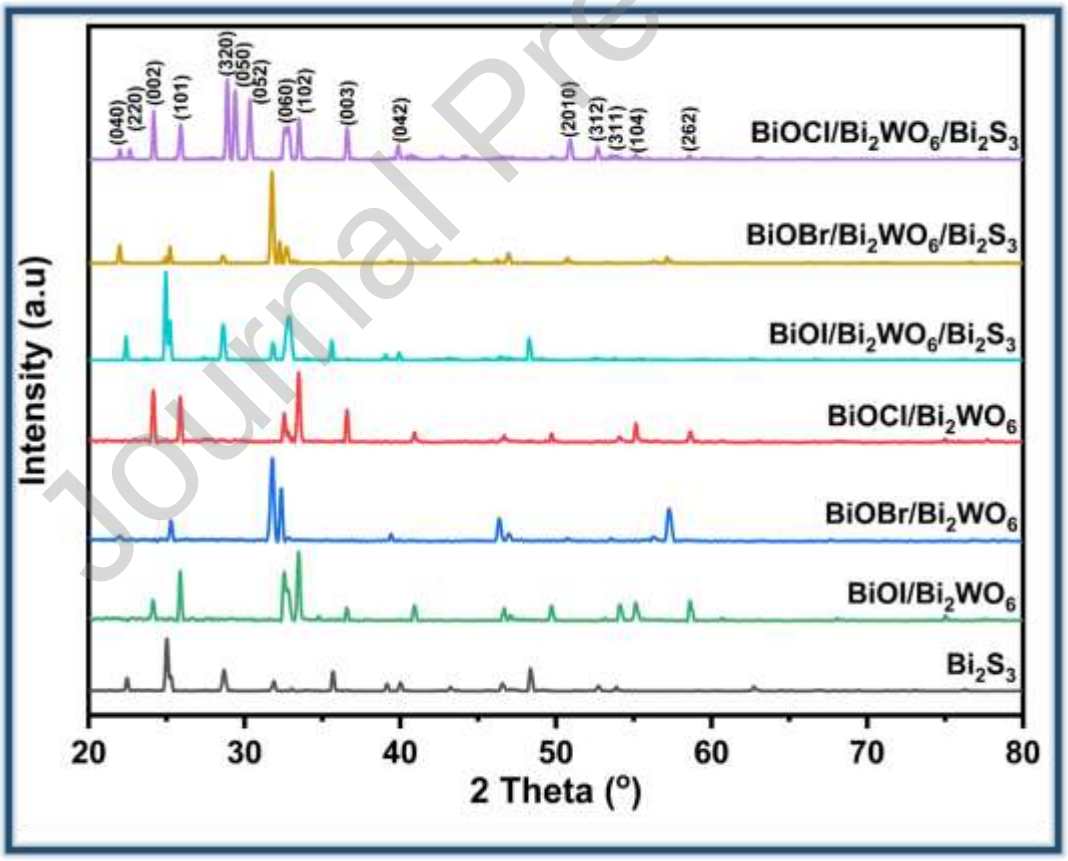

Fig. 2. XRD pattern of Bi_2S_3, binary composites $BiOX/Bi_2WO_6$, and $Bi_2S_3/BiOX/Bi_2WO_6$ heterostructure photocatalysts.

3. Results and discussion

3.1. Structural analysis of the synthesized photocatalysts

The phase analysis and crystallite structures of the prepared heterostructure photocatalysts were examined by powder XRD pattern obtained in the 2θ range from 20 to 80º and the results for pure Bi_2S_3, binary composites of Bi_2WO_6/BiOX, and heterostructure photocatalysts BiOX/Bi_2WO_6/Bi_2S_3 (X = Cl, Br, I) are presented in Fig. 2. The peaks of binary and heterostructure photocatalysts correspond to the respective Bi_2S_3, Bi_2WO_6, and BiOCl, BiOBr, and BiOI compounds. The diffraction peaks of Bi_2S_3 at 25.31, 36.20, 40.63, 43.94, 47.27, 49.95 and 52.61° corresponding to (310), (420), (430), (520), (350), (610), and (061) crystal planes, respectively, correspond to orthorhombic geometry of Bi_2S_3 which is consistent to standard JCPDS No. 01-075-1306 [42]. The diffraction peaks of binary composite BiOCl/Bi_2WO_6 were observed at 24.45, 33.02, 47.44, 55.03, and 56.06° corresponding to (002), (200), (220), (104), and (303), respectively. The crystal planes (002) and (104) are related to the tetragonal geometry of BiOCl (JCPDs No. 01-082-0485) [43], and the crystal planes (200), (220), and (303) present the tetragonal geometry of Bi_2WO_6 (JCPDs No. 00-026-1044) [44]. The characteristic peaks of Bi_2S_3, BiOCl, and Bi_2WO_6 can be observed in the XRD patterns of the Bi_2O_3/BiOCl/Bi_2WO_6 photocatalyst, which does not show any change in the crystal phase. Furthermore, the characteristic peaks of Bi_2S_3, Bi_2WO_6, and BiOBr (JCPDs No. 01-073-2061) [45] can be observed in Bi_2O_3/BiOBr/Bi_2WO_6, and the peaks of Bi_2S_3, Bi_2WO_6, and BiOI (JCPDs No. 00-010-0445) [46] were observed in the XRD pattern of Bi_2O_3/BiOI/Bi_2WO_6.

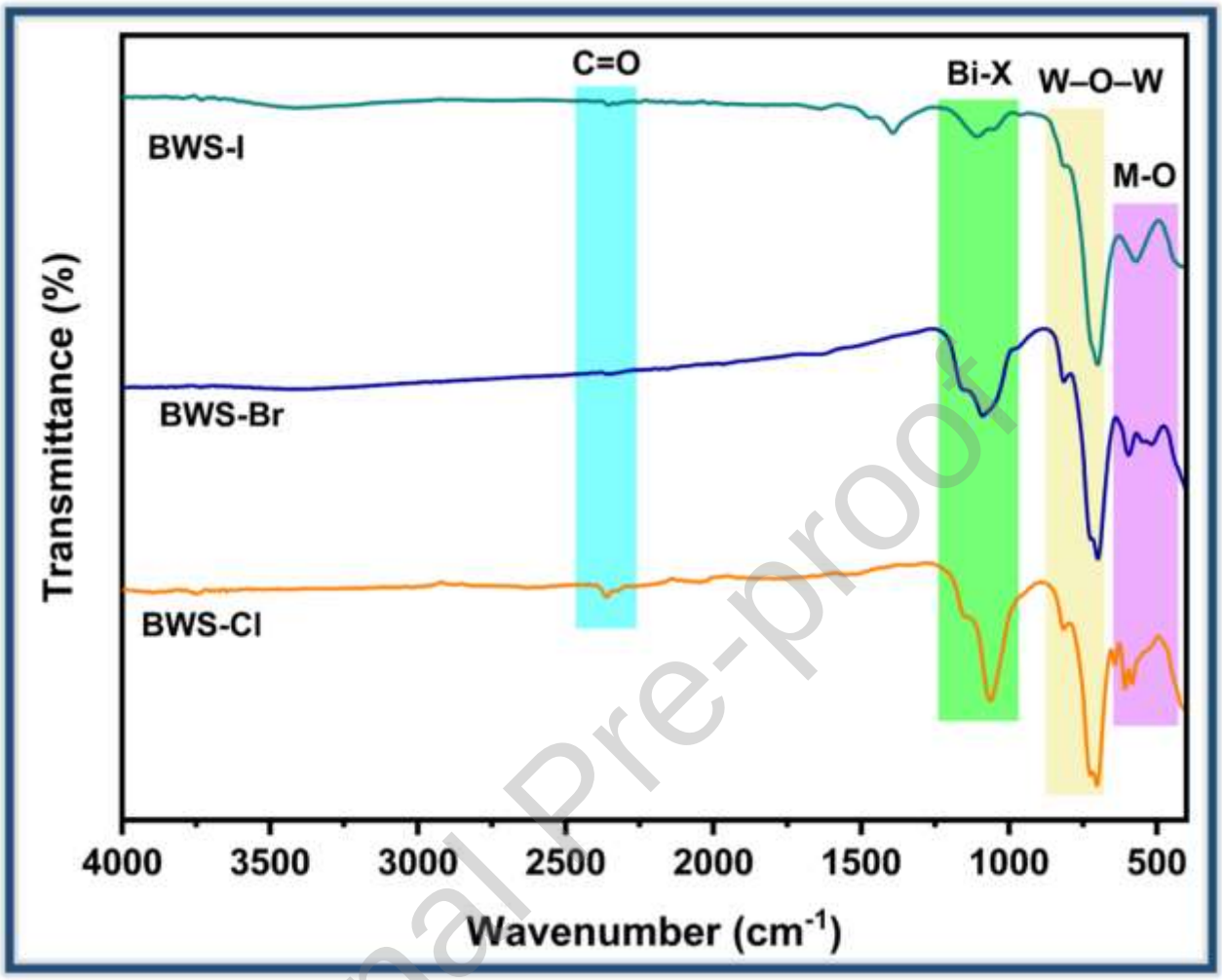

Fig. 3. FTIR spectra of heterostructure photocatalysts.

The composition of as-synthesized Bi_2S_3/BiOX/Bi_2WO_6 can be determined by their bond vibrations observed in the FTIR spectra of heterostructure photocatalysts, BWS-Cl (BiOCl/Bi_2WO_6/Bi_2S_3), BWS-Br (BiOBr/Bi_2WO_6/Bi_2S_3), and BWS-I (BiOI/Bi_2WO_6/Bi_2S_3), as shown in Fig. 3. The broad absorption IR bands at 451 cm^{-1} and 590 cm^{-1} in the IR spectrum of Bi_2S_3/BiOX/Bi_2WO_6 are associated with the Bi–O and W–O, respectively. Additionally, the IR band at 721 cm^{-1} can be associated with the bending and stretching vibrational modes for the W–

O–W bond [47]. A small IR band observed at about 1380 cm^{-1} is due to the vibration of the Bi-X bond [48]. The FTIR spectral analysis indicates the successful synthesis of the photocatalysts.

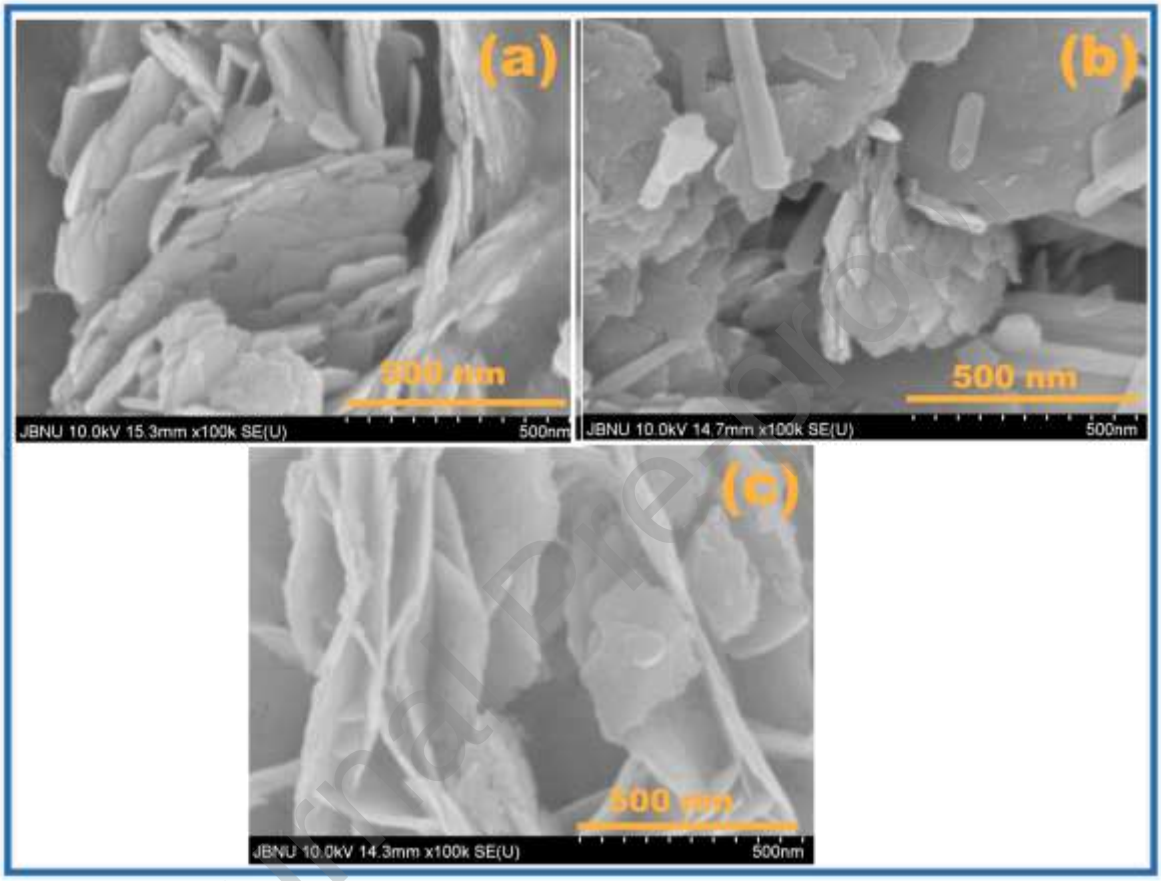

Fig. 4. SEM images of BWO-Cl (a), BWO-Br (b), and BWO-I (c).

3.2.Morphological characteristics

Fig. 4 represents the field-emission scanning electron microscopic (FESEM) images of the synthesized photocatalysts, which show their surface morphology. The heterojunction photocatalysts had mostly entangled flake-like morphology [49]. They show randomly placed irregular-shaped flakes, which are arranged into lamellar, tightly packed formations and

disordered sheet-like structures. The flakes show distinct edges combined with smooth surfaces, but small surface textures are detectable on certain flakes, which might arise from layer formation during growth or from intrinsic crystal elements [50]. Particulate aggregation occurs through flake stacking and overlapping because of both van der Waals interactions and synthesis-related aggregate formation [51].

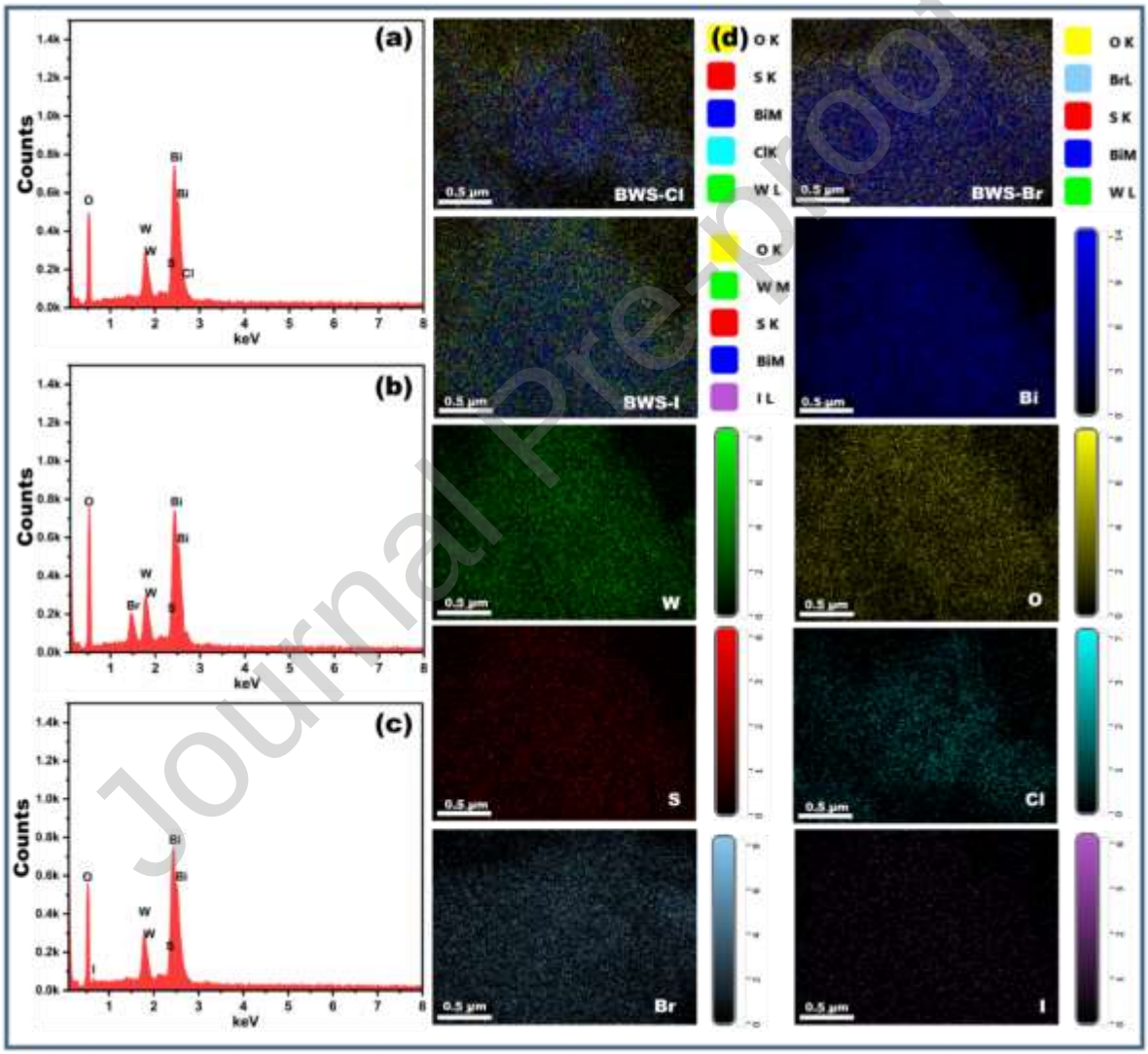

Fig. 5. EDX spectra of BWS-Cl (a), BWS-Br (b), and BWS-I (c), and elemental mapping (d) of various elements of photocatalysts.

The EDX spectra of the photocatalysts show the elemental compositions of the prepared heterostructure photocatalysts (Fig. 5). The EDX spectra show the presence of various elements, such as bismuth (Bi), tungsten (W), oxygen (O), sulfur (S), and chlorine (Cl) in BWS-Cl (a), bromine (Br) in BWS-Br (b), and iodine (I) in BWS-I (c). Fig. 5 (d) shows the distribution of various elements in the photocatalysts, indicating homogeneous distribution of various elements in them, and uniform mixing of BiOX/Bi_2WO_6 with Bi_2S_3.

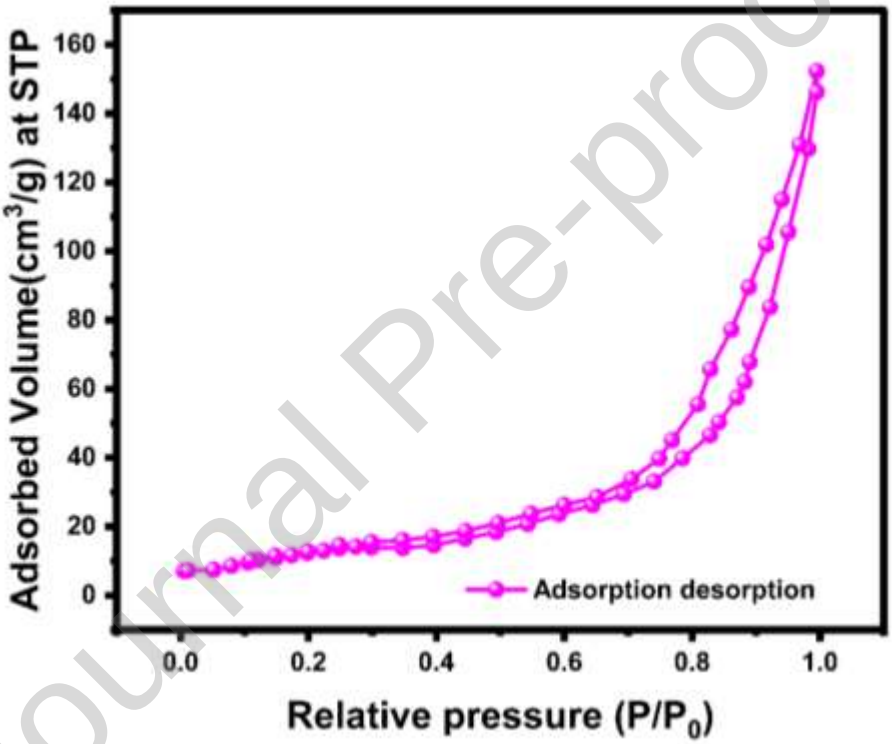

Fig. 6: N_2 adsorption-desorption isotherm by BET analysis

The Brunauer-Emmett Teller (BET) technique was used to analyze the data of the nitrogen adsorption. The BET plot, which was generated after adsorption and desorption against the relative pressure. The plot was very linear, meaning that the interval of pressure used is adequate to apply the BET model. Fig. 6 showed the nitrogen adsorption-desorption isotherm of BWS-Cl exhibited a hysteresis loop at a relative pressure near one, revealing the presence of large

mesopores and macropores, which can be defended as type IV corresponding to IUPAC classification. The BET plot in general suggests a clear adsorption cycle and confirms the accuracy of the computed surface area.

3.3. Optical and spectroscopic studies

Fig. 7 (a–b) shows UV-visible spectra of as-prepared Bi_2S_3, binary composites BiOX/Bi_2WO_6, BWS-Cl, BWS-Br, and BWS-I heterojunction photocatalysts that were recorded from 200 nm to 800 nm wavelength in aqueous suspension to investigate their optical properties. All the photocatalysts exhibited an absorbance peak in the range of 300 nm to 400 nm. However, the absorbance peaks of the photocatalysts shifted slightly to the visible region for BWS-Cl as compared to other BWS-Br and BWS-I, indicating the broadening of the absorption wavelength and the generation of more electron-hole pairs in the case of BWS-Cl, which in turn improved the photocatalytic activity. Optical properties and direct bandgap of the as-prepared BWS-X photocatalysts were calculated using the Tauc's plot, where the absorption coefficient was plotted against the photon energy measured by the following equation for the calculation of the direct band gap value [52]:

$$(\alpha h\nu)^2 = A(h\nu - E_g) \qquad (2)$$

where α is the absorption coefficient, hν is the photon energy, and E_g is the optical band gap value. The as-prepared samples showed the direct band gap of 1.78 eV, 1.89 eV, and 1.94 eV for the BWS-Cl, BWS-Br, and BWS-I heterostructure photocatalysts, respectively.

Furthermore, to understand the light-absorption behavior of binary composites, the bandgap energies of Bi_2S_3 and the as-synthesized binary catalysts were calculated using Tauc's

plots derived from their UV–vis spectra (Fig. 7 b). Bi_2S_3 exhibited a narrow bandgap of 2.04 eV, consistent with its strong absorption in the visible-light region. The binary BiOCl/Bi_2WO_6, BiOBr/ Bi_2WO_6, and BiOI/ Bi_2WO_6 composites showed band gaps of 2.98, 3.05, and 3.11 eV, respectively, reflecting the influence of the halide species on the optical response. These bandgap values correlate well with the observed absorption edges and provide a basis for understanding the enhanced visible-light activity of the ternary heterostructures.

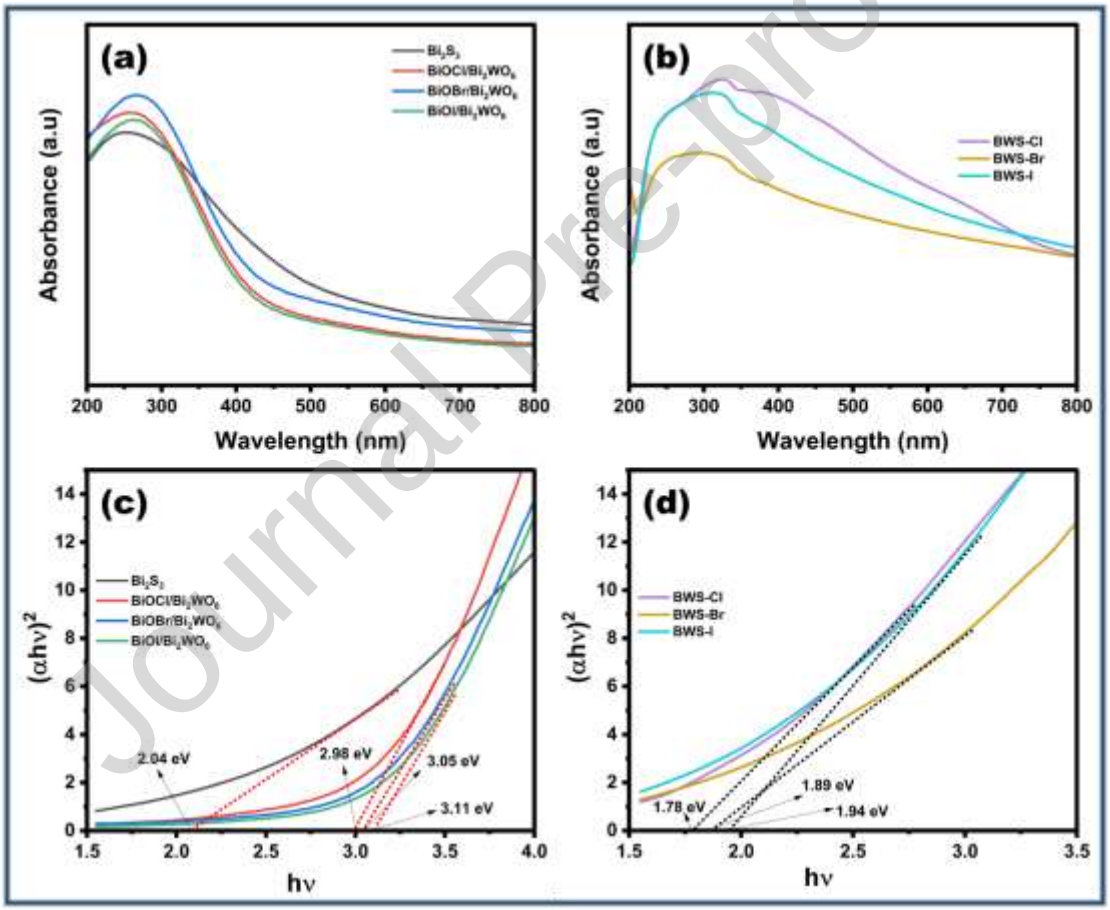

Fig. 7. UV-visible spectra of as-synthesized (a) bismuth sulfide and binary composites (b) ternary heterostructure photocatalysts, (c) Tauc's plots for the measurement of band gap value of Bi_2S_3 and binary composites (d), and band gap of ternary composites BWS-Cl, BWS-Br, and BWS-I.

3.4. Photoluminescence

The synthesized photocatalysts were analyzed by photoluminescence (PL) spectroscopy to assess both electronic and optical properties. PL spectra were recorded using an excitation wavelength of 380 nm. Multiple distinct emission peaks occurred in the range of 400 nm to 800 nm at room temperature, as shown in Fig. 8. Multiple photoluminescence sharp emission peaks at 466, 510, 533, 558, 574, 579, 619, 635, and 655 nm indicate high structural quality and precise electronic transitions. Material crystallinity produces these distinct features when it exists at high levels because it reduces broadening effects and enables distinctive radiative recombination processes. The emission peak that appears around 466 nm could be attributed to intrinsic luminescence, which is due to charge transfer in the hybrid orbital of Bi and O atoms in Bi_2WO_6 [52]. The halogen atoms (Cl, Br, I) lead to a stepwise reduction of PL emission intensity as shown through the color-coded spectra in the order of BWS-I > BWS-Br > BWS-Cl, which shows the limits of electron-hole pair recombination. This behavior decreased intensity and improved charge separation efficiency, resulting in improved photocatalytic performance. Furthermore, the photoelectric properties and transient photocurrent were determined to evaluate the production of current response due to the electron transfer capacity of the photocatalyst by light absorption. The higher the photocurrent, the more the electron transfer during the light absorption, and the better the photocatalytic efficiency [52]. Fig. 9 (a) shows the response of the photocurrent record for BWS-Cl, BWS-Br, and BWS-I, in which the photocurrent density was progressively increased. According to the results of photocurrent, the BWS-Cl heterostructures showed maximum photocurrent, which accelerated the separation and kinetics of the photo-

generated electron. The results reveal that the shorter the semicircle of the curve, the greater the charge transfer efficiency in EIS analysis.

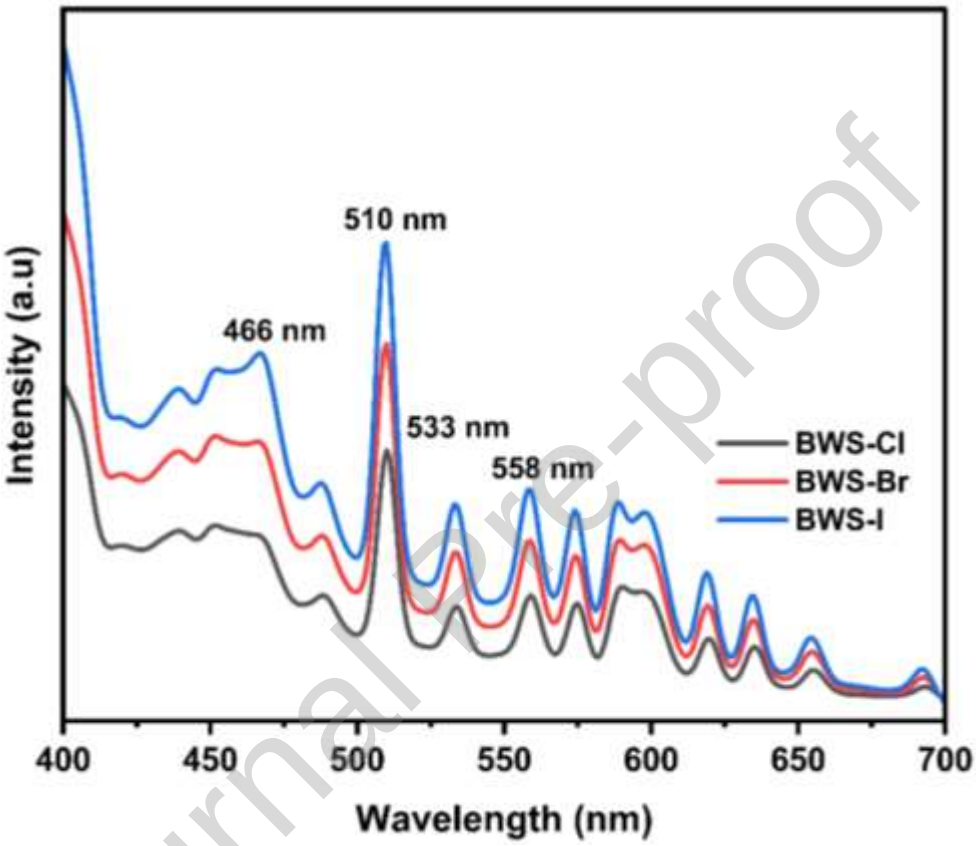

Fig. 8. PL spectra of BWS-Cl, BWS-Br, and BWS-I heterojunction photocatalysts.

Fig. 9 (b) represents the EIS curves of BWS-Cl, BWS-Br, and BWS-I. The radius of the semicircle of BWS-Cl is less than that of BWS-Br and BWS-I, which makes the charge transfer efficiency of BWS-Cl faster. It demonstrates that the heterostructure with chlorine could be useful to enhance the charge transfer capacity of photogenerated electrons and facilitate the separation and migration of photogenerated electrons on the surface of the particle electrode.

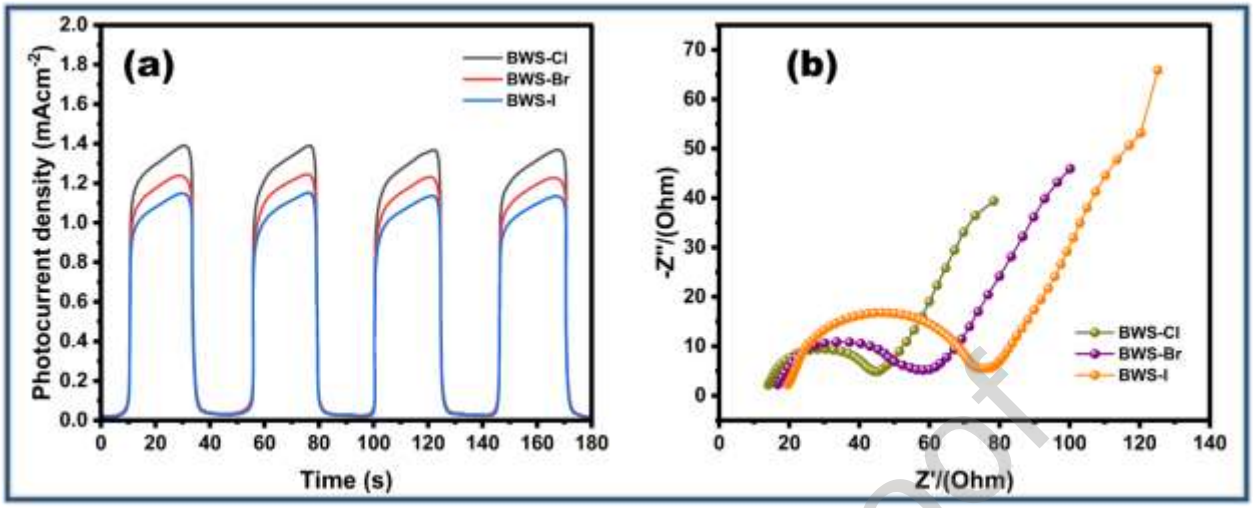

Fig. 9: (a) photocurrent response and (b) EIS measurement of BWS-Cl, BWS-Br, and BWS-I.

3.5. Evaluation of photocatalytic performance

The photocatalytic performance of the synthesized heterostructure photocatalysts BWS-Cl, BWS-Br, and BWS-I was determined by photocatalytic degradation of CFX under sunlight. For the experimental setup, the adsorption–desorption equilibrium of CFX over the photocatalyst was achieved with continuous stirring for 20 min under a dark environment to minimize the absorption effect, and then, the photocatalytic degradation of CFX was carried out under sunlight irradiation with continuous stirring. Fig. 10 (a) shows that the concentration of CFX decreased with an increase in time. Fig. 10 (b) shows that a very minor level degradation of CFX occurred in the absence of photocatalyst, which was only 2% after 2 hours of irradiation. The adsorption of CFX over the BWS-Cl, BWS-Br, and BWS-I photocatalyst observed was 32.78, 33.07, and 43.53%, respectively. The degradation of CFX with heterostructure photocatalysts, BWS-Cl, BWS-Br, and BWS-I, after 120 min was 96.6, 91.0, and 85.9%, respectively. The reaction

kinetics of photodegradation of CFX are well fitted with pseudo-first-order reaction kinetics [53] as shown in Fig. 10 (c), which was determined by the following equation:

$$-Ln(C/C_0) = kt \quad (3)$$

where C_0 is the initial concentration of CFX and C is the concentration of CFX after degradation. The calculated rate constant, "k", for the degradation of CFX over heterostructure photocatalysts BWS-Cl, BWS-Br, and BWS-I was 0.023 min^{-1}, 0.016 $min^{-1,}$ and 0.011 min^{-1}, respectively, as presented in Fig. 10 (d). The degradation efficiency was slightly influenced by the halogen atom present in heterostructure photocatalysts, and maximum degradation of CFX was observed for $BiOCl/Bi_2S_3/Bi_2WO_6$. It is worth noting that some levels of ciprofloxacin removal occurred during the dark adsorption stage, particularly for the ternary composite, which can be attributed to its enhanced surface area, surface charge, and interfacial characteristics. To clearly distinguish adsorption from photocatalytic degradation, all photocatalytic experiments were conducted after reaching adsorption–desorption equilibrium in the dark. Therefore, the subsequent decrease in ciprofloxacin concentration under light irradiation is primarily associated with photocatalytic degradation rather than physical adsorption.

The $BiOX/Bi_2WO_6/Bi_2S_3$ ternary heterostructures exhibited a synergistic effect, which is evident from their high photocatalytic performance. Of the three composites, BWS-Cl showed the highest photodegradation efficiency (96.6% in 120 min), considerably higher than the other two heterostructures, BWS-Br and BWS-I. This tendency can be associated with the increased electronegativity and position of the higher valence band of Cl^-, which increases the oxidative capacity of photogenerated holes [54]. The BWS-Cl showed the highest absorption of CFX under dark conditions, which was 9.8%, and was attracted to more active sites for the subsequent photodegradation reactions, enhancing the photodegradation efficiency. The rate constant of the

apparent reaction (k = 0.023 min^{-1} of BWS-Cl) was by far more active compared to BWS-Br and BWS-I, which means that charge separation was more efficient and generated reactive oxygen species more quickly.

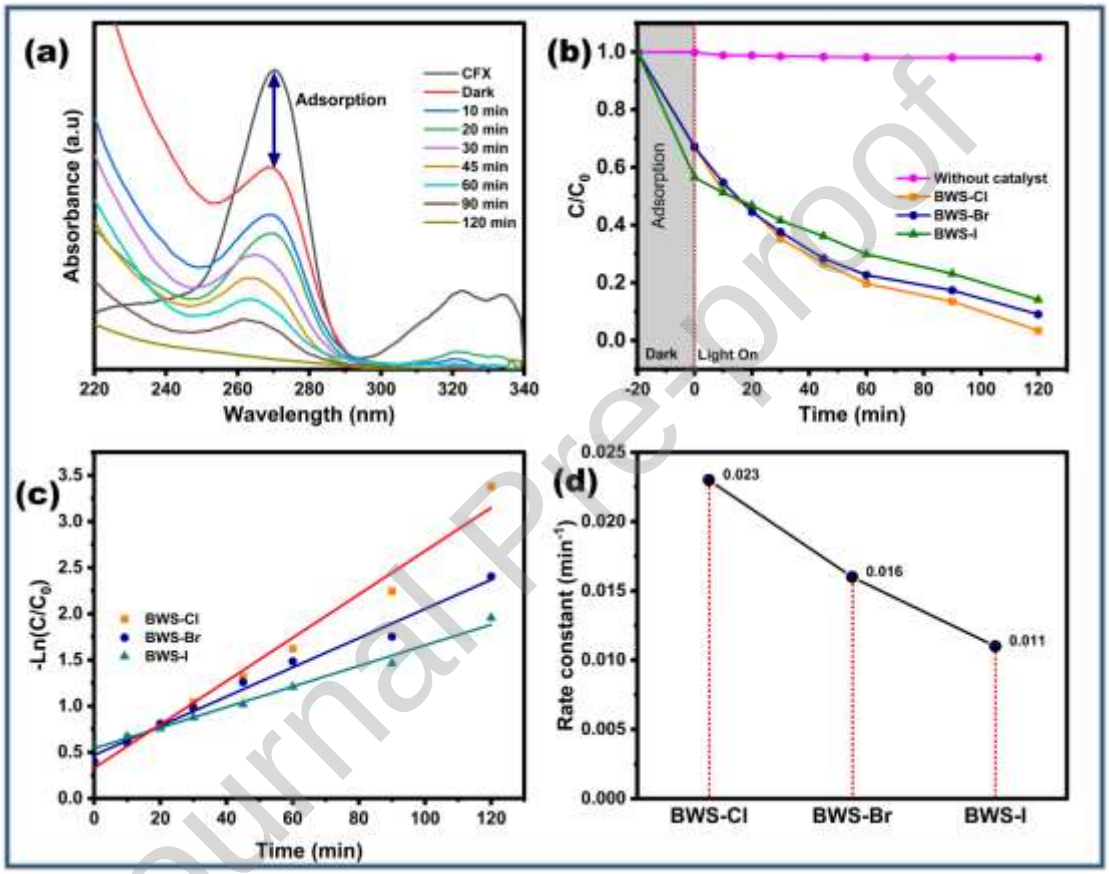

Fig. 10. Graphical presentation of C/C_0 versus time (a), plots of percentage degradation versus time (b), plots of $ln(C/C_0)$ versus time (c) for the degradation of CFX in the presence of heterostructure photocatalysts, BWS-Cl, BWS-Br, and BWS-I, and UV-Visible spectra for the degradation of CFX with time for BWS-Cl (d).

The complementary nature of the various components of the ternary heterostructures explains the improved performance of the ternary composites. For example, Bi_2S_3, due to its narrow

bandgap, can efficiently capture visible photons and provide electrons, and Bi_2WO_6 can provide powerful oxidative holes. The addition of BiOX also facilitates the charge migration and interfacial electron transfer because of its layered structure and internal electric field. Such a multi-component system allows an effective S-scheme charge-transfer pathway, which is confirmed by band-position computations and radical-trapping findings. Throughout this process, the highly reduced electrons of Bi_2S_3 and the highly oxidizing holes of BiOCl are maintained, allowing the creation of O_2^- and h+ as the most prevalent reactive species. These species continuously attack the quinolone ring and functional groups of ciprofloxacin, leading to rapid degradation in natural sunlight. In general, improved kinetics, expanded light absorption, and improved charge transfer are the combination of excellent photocatalytic activity of the ternary heterostructures relative to their binary and single counterparts.

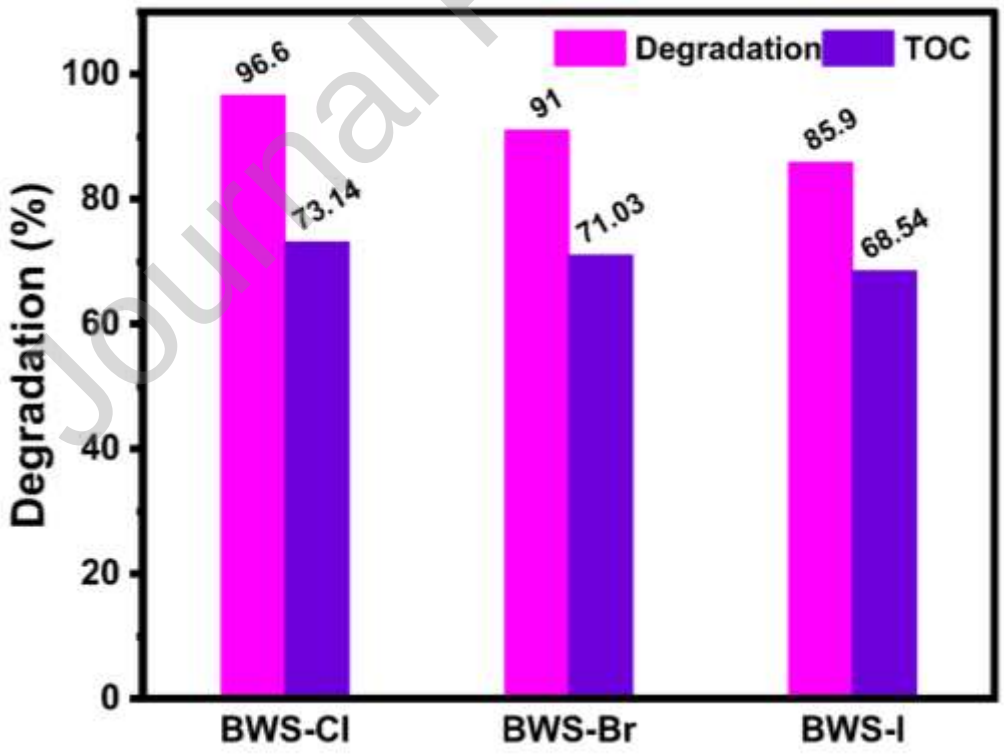

Fig. 11: Comparative results of degradation and TOC removal.

The photocatalytic degradation was carried out under natural sunlight to test the mineralization capacity of these ternary heterostructures by total organic carbon (TOC) analysis. The mineralization efficiency of the BWS-Cl composite was the best with 73.14% removal of TOC in 120 min, but the other two heterostructures, BWS-Br and BWS-I, also showed high mineralization efficiency, 71.03 and 68.54% respectively, as shown in Fig. 11. The high mineralization efficiency indicates that these photocatalysts are not only active in the degradation of the chromophore structure of CFX but also able to oxidize the intermediate species of the photocatalyst to mineral end-products. The high correlation between the reduction of TOC and the photodegradation trend also confirms the amplified charge separation and effective oxidative activity of the BWS-Cl heterostructure.

3.5.1. Optimization of the different parameters for photocatalytic activity

The photocatalytic efficiency of the heterostructure photocatalysts for the degradation of CFX depends on three factors: the initial concentration of CFX, catalyst dose, and the pH of the CFX solution. Different experimental arrangements were made to determine the best reaction conditions for the degradation of CFX. Fig. 12 (a) illustrates that among various catalysts, the degradation efficiency of CFX becomes more efficient when the catalyst dosage is increased from 0.2 g/L to 0.6 g/L, and maximum degradation was achieved with a 0.6 g/L dose of photocatalyst. Further increase in catalyst dosage, more than 0.6 g/L, decreased the production of photoinduced carrier, leading to reduced efficiency because an extra dose of photocatalyst made the reaction medium turbid and less effective because of the reduced light absorption. The optimum dosage of photocatalyst was found to be 0.6 g/L for achieving the maximum

degradation efficiency. Fig. 12 (b) shows the degradation results of CFX with different initial concentrations of CFX while keeping the constant optimal dose of photocatalyst. When the CFX solution concentration rises from 2.5 to 5 ppm, it does not affect the degradation of CFX, and maximum degradation was obtained at a 5 ppm concentration of CFX.

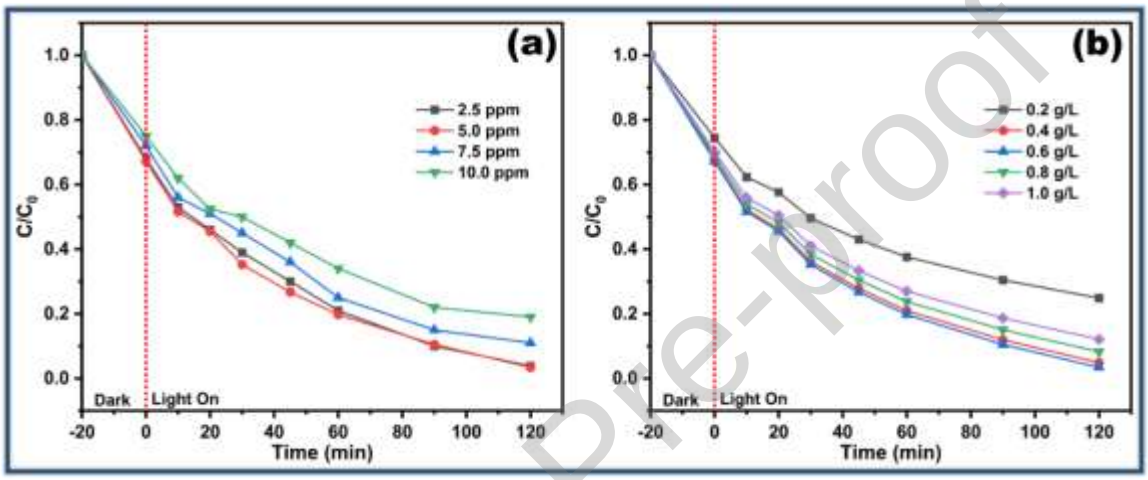

Fig. 12. Effects of initial CFX concentration (a) and catalyst dose (b) on the degradation of CFX over BWO-Cl heterostructure photocatalysts.

When the initial concentration of CFX increased from 5 ppm, a significant decrease in the photocatalytic degradation of CFX was observed. When the concentration of CFX rises in the system, the CFX molecules bind to active sites of the surface of the photocatalyst and form their intermediates, which negatively affect the absorption of light, thus reducing CFX degradation.

3.5.2. Effect of initial pH of test solution and point of zero charge

The chemical nature of drug solutions, such as acidic or basic, determines how photocatalysts work during pollutant decomposition. The interaction of CFX with the surface of photocatalysts and CFX photodegradation depends heavily on the initial pH of the CFX solution. The

photocatalytic degradation of CFX with a concentration of 5 ppm solution containing 0.4 g/L catalyst dose under sunlight was conducted for 2 h at various initial pHs, such as 3, 5, 7, 9, and 11. The initial pH of the CFX solution was adjusted with 0.2 N HCl and 0.1 N NaOH solutions. Fig. 13 (a) shows the degradation efficiency of CFX at various pH values.

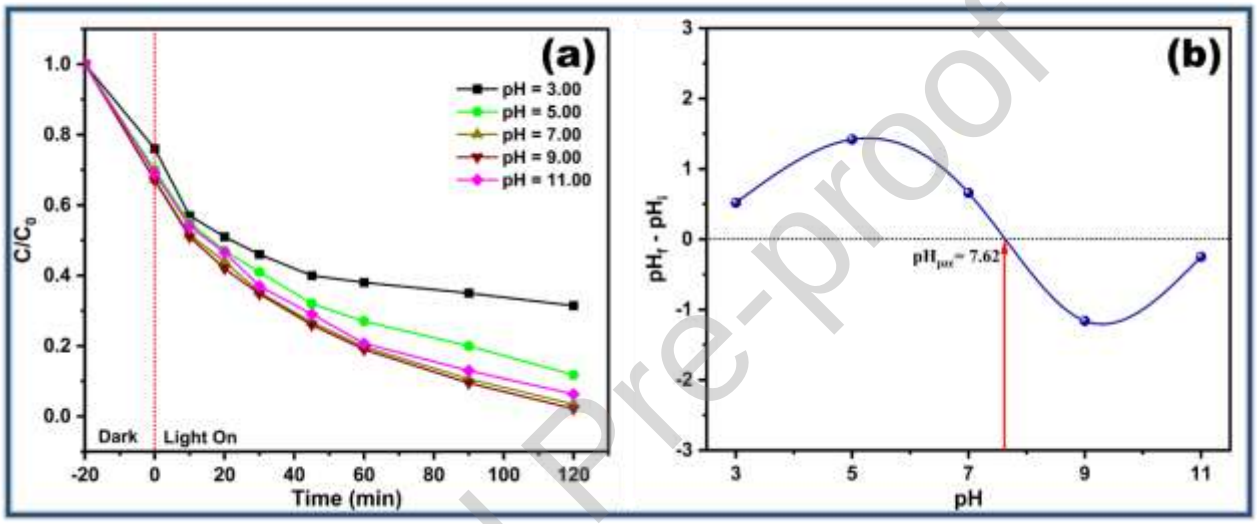

Fig. 13. Influence of pH value of drug solution on photocatalytic performance (a), and pH for the point zero charge value of photocatalyst (b).

The interaction between CFX molecules and the photocatalyst surface depends on both the chemical states of CFX at various pHs and the point zero charge pH (pHpzc) value of the photocatalyst [55]. The adsorption behavior of CFX on the surface of the photocatalyst is affected by the dissociation constant values of CFX, which are pKa1= 6.1 and pKa2 = 8.7, i.e., the electrostatic attraction between CFX and photocatalysts is the highest at pH 6.1 and the lowest at pH 8.7. The photocatalyst showed the experimental pHpzc value at pH 7.62, and at pH below the pHpzc, the surface of the photocatalysts attains a positive charge, and above attains a negative charge. The interaction between the negatively-charged $–COO^-$ group of CFX and the

positively charged surface of photocatalysts occurs at pH 6.1 because the negatively charged CFX is attracted by the positively charged photocatalyst via electrostatic forces [56]. The absorption of CFX by the photocatalyst decreases above pH 7.62 due to electrostatic repulsion as the surface of both the photocatalyst and CFX becomes negative. However, Fig. 13(a) shows that the maximum degradation of CFX occurred at pH 9.00, when the surface of the photocatalyst and CFX both become negative. The results suggest that, instead of facilitating, electrostatic attraction between the photocatalysts and CFX hinders the degradation of the latter [57]. Therefore, the optimum pH for the photocatalytic degradation of CFX by the developed heterostructures is 9.0, when the repulsive forces between the photocatalyst and CFX are the highest.

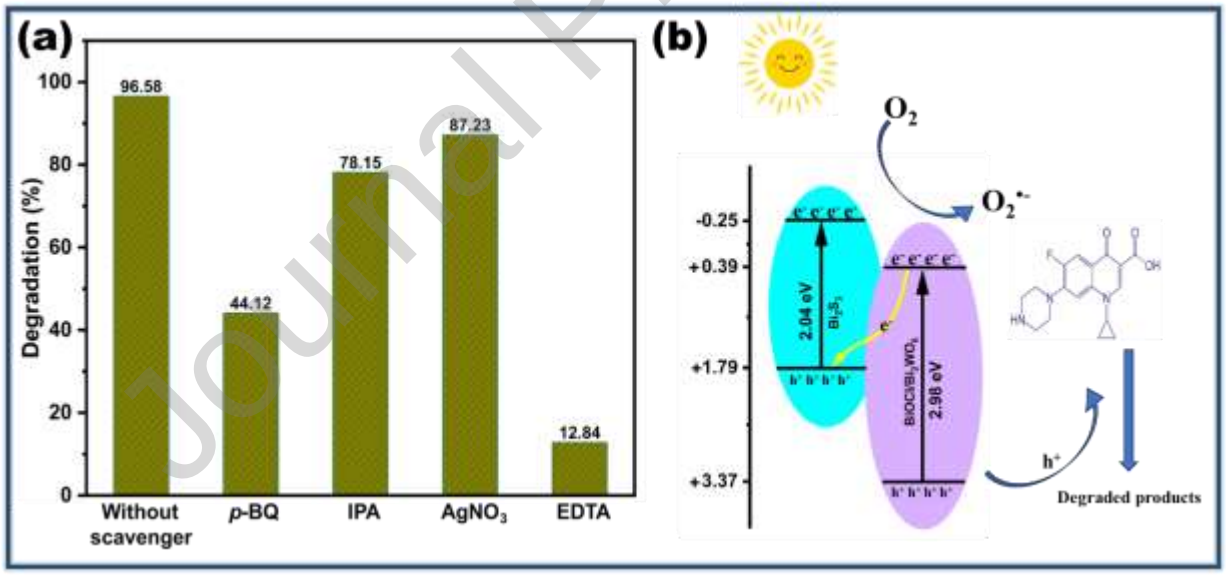

Fig. 14: Effect of scavengers on photocatalytic reaction (a), and reaction mechanism of photocatalysis (b).

3.5.3. Radical scavenging and mechanism

The organic pollutant degradation by photocatalytic processes involves mainly four types of reactive species, such as electrons (e^-,), holes (h^+), and hydroxyl (OH) and superoxide (O_2^-) radicals [52]. Experiments were conducted to find the dominant active species during the degradation of aqueous CFX solution using a photocatalyst under its established optimal conditions. Tests were conducted using isopropanol, para-benzoquinone, EDTA, and silver nitrate as OH and $\bullet O_2^-$, h^+, and electron-trapping agents, respectively. The level of photocatalytic inhibition that occurs in the presence of these scavenging agents demonstrates which reactive species are most significant for overall degradation, as shown in Fig. 14 (a). The impact of isopropanol and silver nitrate scavengers on degradation is minimal when compared to other trapping agents. Use of EDTA as an h^+ scavenger and p-BQ as $\bullet O_2^-$ scavenger resulted in reduced photocatalytic degradation of CFX from 96.56 to 12.84% and 44.12%, respectively, which is evidence that h^+ and $\bullet O_2^-$ are the main active species in the photocatalytic degradation of CFX [58]. To quantitatively support the proposed S-scheme charge-transfer pathway, the valence band (VB) and conduction band (CB) edge potentials for the optimized BWS-Cl photocatalyst were estimated using the Mulliken electronegativity method. To elucidate the charge transfer behavior in the $BiOCl/Bi_2WO_6/Bi_2S_3$ ternary system, an S-scheme-like heterojunction mechanism is proposed. In this system, Bi_2S_3 was coupled with a pre-formed $BiOCl/Bi_2WO_6$ binary heterojunction. Therefore, the $BiOCl/Bi_2WO_6$ component can be regarded as an integrated oxidation photocatalyst unit. The band edge positions of Bi_2S_3 and the $BiOCl/Bi_2WO_6$ binary composite were estimated using the Mulliken electronegativity method according to $E_{CB} = X - E_e - 0.5E_g$ and $E_{VB} = E_{CB} + E_g$, where X is the absolute electronegativity, and E_e is the energy of free electrons on the hydrogen scale (4.5 eV). For Bi_2S_3 (E_g = 2.04 eV), the CB and VB potentials were calculated to be −0.25 and +1.79 eV vs NHE, respectively. For the

$BiOCl/Bi_2WO_6$ binary heterojunction (E_g = 2.98 eV), the CB and VB potentials were estimated to be +0.39 and +3.37 eV vs NHE. Under solar light irradiation, both components are photoexcited. The photogenerated electrons in the conduction band of the $BiOCl/Bi_2WO_6$ tend to recombine with the holes in the valence band of Bi_2S_3 at the interface. This selective recombination pathway follows an S-scheme-like charge transfer mechanism, which effectively retains charge carriers with strong redox ability. The preserved electrons and holes, therefore, possess strong reducing and oxidizing ability, respectively, which explains the experimental observation of enhanced reactive-species generation and superior photocatalytic activity of BWS-Cl. It should be noted that the band edge positions discussed above were estimated using the Mulliken electronegativity method, which provides an approximate evaluation of energetic alignment. As this approach does not account for interfacial effects, defect states, or experimental band bending in composite systems, the absolute values should be interpreted with caution. Therefore, the calculated band positions are used primarily to support a qualitative understanding of the charge transfer pathway rather than to assert precise energetic alignment.

3.6. Reusability and stability

For practical usage, catalysts should be stable and reusable many times, which leads to extra economic value and superior environmental outcomes. The heterojunction photocatalysts synthesized in this work provided outstanding photocatalytic degradation of CFX, and reusability was studied up to five cycles, as shown in Fig. 15. The BWS-Cl photocatalyst maintained consistent degradation efficiency up to five cycles, with a small decline in photodegradation efficiency from 96.6 to 92.9% after five cycles, showing its high stability. The heterostructure

photocatalysts demonstrated high potential for practical use as they can be recovered and separated from suspension simply by filtration.

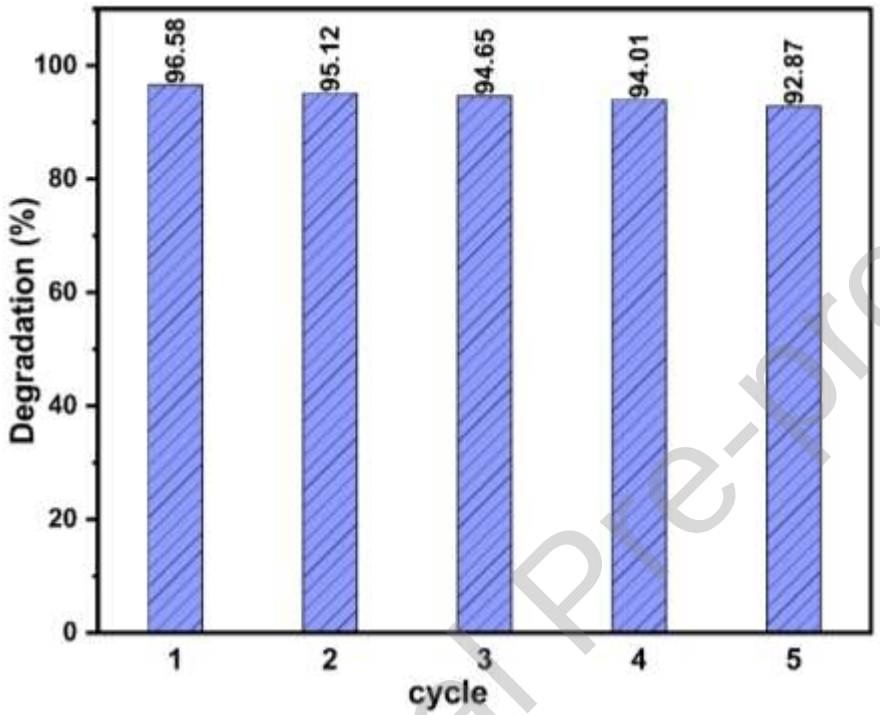

Fig. 15: Photocatalytic efficiency after multiple uses of heterostructure photocatalysts, BWS-Cl.

3.7.Comparison of photocatalytic degradation performance with other heterostructures

Table 1 shows the comparison of photocatalytic degradation performance of heterojunction photocatalysts developed in this work for the photodegradation of CFX with several similar heterojunction photocatalysts studied by others for the photodegradation of CFX and other organic contaminants (39,59–65). Of them, $Fe_2O_3/Bi_2O_3/ZnO$ [59] and g-C_3N_4 or Bi/BiOBr [61] showed the lowest CFX degradation efficiency, 83.0 and 84.9% respectively. Comparatively,

Table 1. Photocatalytic degradation performance of various heterojunction photocatalysts for the removal of CFX and other organic pollutants.

Photocatalysts	Pollutants	Reaction conditions				Degradation efficiency (%)	Ref.
		Pollutant conc. (ppm)	catalyst loading (g/L)	Treatment time (min)	Light source		
Cu_3SnS_4/L-BiOBr	CFX	20	0.5	180	300 W Xe	93.0	[60]
BiOCl/$Bi_{12}O_{17}Cl_2$/Bi_2O_3	CFX	15	1.0	60	300 W Xe	95.2	[39]
Fe_2O_3/Bi_2O_3/ZnO	CFX	10	0.2	70	300W Xe	83.0	[59]
g-C_3N_4 or Bi/BiOBr	CFX	20	0.2	30	150W Xe	84.9	[61]
Bi_2S_3/$BiVO_4$/g-C_3N_4	TC	10	0.5	90	visible light	80.7	[62]
BiOBr/Bi_2S_3/CdS	MB	10	1.0	120	150 W halogen	83.3	[63]
Ag_2S/AgI-Bi_2S_3/BiOI	SA	10	1.5	360	300 W Xe	89.2	[34]
BiOCl/Bi_2MoO_6/Bi_2O_3	CFX	5	0.5	180	200 W tungsten	90.8	[64]
Gd^{3+}-doped $Bi_4O_5I_2$	CFX	10	0.4	120	300 W Xe	94.5	[65]
BiOCl/Bi_2WO_6/Bi_2S_3	CFX	5	0.6	120	200 W tungsten	96.6	This Work
BiOBr/Bi_2WO_6/Bi_2S_3						91.0	
BiOI/Bi_2WO_6/Bi_2S_3						85.9	

similar bismuth oxide-based photocatalysts, such as Bi_2S_3/$BiVO_4$/g-C_3N_4 [62] and BiOBr/Bi_2S_3/CdS [63], showed 80.7% and 83.3% photodegradation of TC and MB, respectively. BiOBr/Bi_2S_3/CdS can release Cd into treated water, which is a possible carcinogen. The CFX degradation by different heterojunction photocatalysts ranged from 80.7 to 95.6% [39,60–65]. On the other hand, Mn_2O_3/Mn_3O_4/MnO_2, BiOCl/$Bi_{12}O_{17}Cl_2$/Bi_2O_3, and Gd^{3+}-doped $Bi_4O_5I_2$ photocatalysts showed very good degradation of CFX, and the photodegradation efficiency reached 95.6, 95.2, and 94.5%, respectively. In comparison, our developed

heterojunction photocatalyst $BiOCl/Bi_2WO_6/Bi_2S_3$ exhibited excellent photodegradation of CFX, which reached 96.6%. It should be emphasized that the degradation efficiency of various photocatalysts reported here was obtained under different experimental conditions, including variations in initial pollutant concentration, catalyst dosage, irradiation time, pH, and light source. Therefore, a precise quantitative comparison is not feasible, and the comparison should be regarded as indicative rather than absolute. Despite these differences, the present ternary photocatalyst demonstrates competitive photocatalytic activity for CFX degradation, achieving 96.6% removal under the mentioned experimental conditions. Compared with other Bi-based heterostructures listed in Table 1, the performance of the $BiOCl/Bi_2WO_6/Bi_2S_3$ falls within or above the upper range of reported degradation efficiencies, even when considering differences in catalyst loading and irradiation conditions. This enhanced activity can be attributed to the synergistic effect of the S-scheme-like charge transfer pathway and improved adsorption–photocatalysis coupling, which collectively facilitate efficient charge separation and utilization under solar-light irradiation.

4. Conclusions

In this study, we successfully synthesized a series of heterostructure photocatalysts, including ($BiOBr/Bi_2WO_6/Bi_2S_3$, $BiOCl/Bi_2WO_6/Bi_2S_3$, and $BiOI/Bi_2WO_6/Bi_2S_3$) by the hydrothermal process followed by calcination. The heterostructure photocatalyst $BiOCl/Bi_2WO_6/Bi_2S_3$ (96.6%) showed significantly higher photocatalytic performance compared to $BiOBr/Bi_2WO_6/Bi_2S_3$ (91.0%) and $BiOI/Bi_2WO_6/Bi_2S_3$ (85.9%). The lowest electrons/holes pair recombination, as evident by PL analysis, supported the highest photocatalytic efficiency of the

$BiOCl/Bi_2WO_6/Bi_2S_3$. The optimum conditions for the maximum CFX degradation were pH = 7–9, a 5ppm solution of CFX, and a catalyst dose of 0.6 g/L. The trapping experiment showed that the h^+ and $\bullet O_2$ were the main active species in the degradation of CFX by the $BiOX/Bi_2WO_6/Bi_2S_3$heterostructure photocatalysts. The fabricated heterostructure photocatalysts exhibited excellent stability throughout drug degradation processes, making them a promising candidate for practical applications in environmental remediation.

Outlook

This article reveals that $BiOX/Bi_2WO_6/Bi_2S_3$ ternary heterostructures can potentially be used for the visible-light photocatalytic degradation of CFX; nevertheless, several limitations of visible-light photocatalysts need to be considered. The seasonal variations, cloudy days, and the change in atmospheric temperature may cause the fluctuation of the intensity and spectral distribution of solar irradiation and variability in the performance of photocatalysts. Although the experiments were conducted at similar solar conditions, long-term experiments under various climatic conditions need to be conducted to ascertain the stability and reliability of the photocatalysts for practical applications.

Future research should include the assessment of photocatalytic performance of the developed heterostructures under controlled simulated-sunlight to supplement the data of natural sunlight and to decouple the effect of irradiance variation. Further studies are also required to learn how photocatalysts work in real wastewater matrices, where other ions and natural organic matter can compete with performance. Adding more sophisticated characterizations, like the determination of intermediate products, prolonged studies of mineralization, and electrochemical analysis,

would provide additional information about the degradation pathway and the charge-transfer mechanism. Furthermore, the immobilization of photocatalysts on various solid supports or the incorporation of the photocatalysts into fixed-bed solar reactors will make their recovery from the treated water easier. In the long term, it is possible to optimize the band structure to increase charge isolation under dark conditions, increase recyclability, and create scalable solar-driven treatment systems, which are promising paths to improve these materials by allowing their use in real-world water purification processes.

CRediT authorship contribution statement

Muhammad Naeem: Conceptualization, Investigation, Writing – original draft. **Muhammad Imran:** Resources, Supervision. **Shoomaila Latif:** Methodology, Writing – review & editing Resources. **Adnan Ashraf:** Formal analysis. **Mohammad Mahbubul Hassan:** Validation, Writing – review & editing, **Muhammad Naeem Khan:** Writing – review & editing.

Declaration of Competing Interest

The authors declare that they have no known competing financial interests or personal relationships that could have appeared to influence the work reported in this paper.

Data availability

The raw data used in this work are available on request.

References

[1] D.G.J. Larsson, C.-F. Flach, Antibiotic resistance in the environment, Natur. Rev. Microbiol. 20 (2021) 257–269. DOI: https://doi.org/10.1038/s41579-021-00649-x

[2] S.A. Kraemer, A. Ramachandran, G.G. Perron, Antibiotic pollution in the environment: From microbial ecology to public policy, Microorganisms 7 (2019) 180. DOI: https://doi.org/10.3390/microorganisms7060180

[3] Y. Wang, X. Dong, J. Zang, X. Zhao, F. Jiang, L. Jiang, C. Xiong, N. Wang, C. Fu, Antibiotic residues of drinking-water and its human exposure risk assessment in rural Eastern China, Water Res. 236 (2023) 119940. DOI: https://doi.org/10.1016/j.watres.2023.119940

[4] M.A. Qamar, M. Javed, S. Shahid, Designing and investigation of enhanced photocatalytic and antibacterial properties of 3d (Fe, Co, Ni, Mn and Cr) metal-doped zinc oxide nanoparticles, Optic. Mater. 126 (2022) 112211. DOI: https://doi.org/10.1016/j.optmat.2022.112211

[5] R.J. Alves Felisardo, E. Brillas, L.F. Romanholo Ferreira, E.B. Cavalcanti, S. Garcia-Segura, Degradation of the antibiotic ciprofloxacin in urine by electrochemical oxidation with a DSA anode, Chemosphere 344 (2023) 140407. DOI: https://doi.org/10.1016/j.chemosphere.2023.140407

[6] R.R. Chandrapal, K. Bharathi, G. Bakiyaraj, S. Bharathkumar, Y. Priyajanani, S. Manivannan, J. Archana, M. Navaneethan, Harnessing $ZnCr_2O_4$/g-C_3N_4 nanosheet heterojunction for enhanced photocatalytic degradation of Rhodamine B and

ciprofloxacin, Chemosphere 350 (2024) 141094. DOI: https://doi.org/10.1016/j.chemosphere.2023.141094

[7] A. Sheikhmohammadi, E. Asgari, B. Hashemzadeh, Photo-catalytic degradation of ciprofloxacin by UV/ZnO/SO_3 process: performance, kinetic, degradation pathway, energy consumption and total cost of system, Int. J. Environ. Anal. Chem. 103 (2023) 5296–5310. DOI: https://doi.org/10.1080/03067319.2021.1937616

[8] X. Yu, J. Zhang, J. Zhang, J. Niu, J. Zhao, Y. Wei, B. Yao, Photocatalytic degradation of ciprofloxacin using Zn-doped Cu_2O particles: Analysis of degradation pathways and intermediates, Chem. Eng. J. 374 (2019) 316–327. DOI: https://doi.org/10.1016/j.cej.2019.05.177

[9] M. Sher, S.A. Khan, S. Shahid, M. Javed, M.A. Qamar, A. Chinnathambi, H.S. Almoallim, Synthesis of novel ternary hybrid g-C_3N_4@ Ag-ZnO nanocomposite with Z-scheme enhanced solar light-driven methylene blue degradation and antibacterial activities, J. Environ. Chem. Eng. 9 (2021) 105366. DOI: https://doi.org/10.1016/j.jece.2021.105366

[10] W. Qi, Z. Cheng, S. Liu, M. Yang, Emerging transition metal nitrides in solar energy conversion: design strategies and future perspectives for efficient photocatalysis, Catal. Sci. Technol. 13 (2023) 6864–6877. DOI: https://doi.org/10.1039/D3CY01097J

[11] M.A. Qamar, S. Shahid, M. Javed, Synthesis of dynamic g-C_3N_4/Fe@ ZnO nanocomposites for environmental remediation applications, Ceramic. Int. 46 (2020) 22171–22180. DOI: https://doi.org/10.1016/j.ceramint.2020.05.294

[12] K.S. Kumar, K. Vaishnavi, P. Venkataswamy, G. Ravi, K. Ramaswamy, M. Vithal, Photocatalytic degradation of methylene blue over N-doped $MnWO_4$ under visible light

irradiation, J. Indian Chem. Soc. 98 (2021) 100140. DOI: https://doi.org/10.1016/j.jics.2021.100140

[13] M. Arumugam, S.J. Lee, T. Begildayeva, S.S. Naik, Y. Yu, H. Lee, J. Theerthagiri, M.Y. Choi, Enhanced photocatalytic activity at multidimensional interface of 1D-Bi_2S_3@2D-GO/3D-BiOI ternary nanocomposites for tetracycline degradation under visible-light, J. Hazard. Mater. 404 (2021) 123868. DOI: https://doi.org/10.1016/j.jhazmat.2020.123868

[14] J. Zhao, Z. Zhao, N. Li, J. Nan, R. Yu, J. Du, Visible-light-driven photocatalytic degradation of ciprofloxacin by a ternary Mn_2O_3/Mn_3O_4/MnO_2 valence state heterojunction, Chem. Eng. J. 353 (2018) 805–813. DOI: https://doi.org/10.1016/j.cej.2018.07.163

[15] M.A. Qamar, S. Shahid, M. Javed, M. Shariq, M.M. Fadhali, O. Madkhali, S.K. Ali, I.S. Syed, M.Y. Awaji, M. Shakir Khan, Accelerated decoloration of organic dyes from wastewater using ternary metal/g-C_3N_4/ZnO nanocomposites: an investigation of impact of g-C_3N_4 concentration and Ni and Mn doping, Catalysts 12 (2022) 1388. DOI: https://doi.org/10.3390/catal12111388

[16] D. Liu, L. Jiang, D. Chen, Z. Hao, B. Deng, Y. Sun, X. Liu, B. Jia, L. Chen, H. Liu, Photocatalytic self-Fenton degradation of ciprofloxacin over S-scheme $CuFe_2O_4$/$ZnIn_2S_4$ heterojunction: Mechanism insight, degradation pathways and DFT calculations, Chem. Eng. J. 482 (2024) 149165. DOI: https://doi.org/10.1016/j.cej.2024.149165

[17] M. Javed, M.A. Qamar, S. Shahid, H.O. Alsaab, S. Asif, Highly efficient visible light active Cu–ZnO/S-gC_3N_4 nanocomposites for efficient photocatalytic degradation of organic pollutants, RSC Adv. 11 (2021) 37254–37267. DOI: https://doi.org/10.1039/D1RA07203J

[18] S.S. Hassan, M. Javed, M.N. Akhtar, M.A. Qamar, N. Ahmed, M. Saeed, K. Aroosh, S. Khan, S. Asif, The photocatalytic and antibacterial potential of highly efficient S-scheme binary S-gC_3N_4@ Co-zinc ferrite nanocomposite, Optic. Mater. 142 (2023) 114046. DOI: https://doi.org/10.1016/j.optmat.2023.114046

[19] S. Zhang, X. Ou, Q. Xiang, S.A. Carabineiro, J. Fan, K. Lv, Research progress in metal sulfides for photocatalysis: From activity to stability, Chemosphere 303 (2022) 135085. DOI: https://doi.org/10.1016/j.chemosphere.2022.135085

[20] Z. Li, S. Chen, Z. Li, J. Sun, J. Yang, J. Wei, S. Wang, H. Song, Y. Hou, Visible light driven antibiotics degradation using S-scheme Bi_2WO_6/$CoIn_2S_4$ heterojunction: Mechanism, degradation pathways and toxicity assessment, Chemosphere 303 (2022) 135113. DOI: https://doi.org/10.1016/j.chemosphere.2022.135113

[21] A.A.P. Khan, M. Nazim, A.M. Asiri, Efficient catalytic degradation of organic pollutants with cupric oxide nanomaterials in aqueous medium, J. Environ. Chem. Eng. 9 (2021) 106305. DOI: https://doi.org/10.1016/j.jece.2021.106305

[22] T. Yuan, J. Gu, S. Wang, S. Lu, Y. Liu, H. Bi, F. Jiang, H. Chen, P-doped bismuth sulfide for improved photocatalytic degradation of bisphenol A: Role of built-in electric field and S vacancies, J. Cleaner Prod. 434 (2024) 140159. DOI: https://doi.org/10.1016/j.jclepro.2023.140159

[23] J. Ding, C. Li, H. Yin, Y. Zhou, S. Wang, K. Liu, J. Wang, One-pot solvothermal synthesis of Bi/Bi_2S_3/Bi_2WO_6 S-scheme heterojunction with enhanced photoactivity towards antibiotic oxytetracycline degradation under visible light, Environ. Pollut. 327 (2023) 121550. DOI: https://doi.org/10.1016/j.envpol.2023.121550

[24] S. Selvi, R. Rajendran, N. Jayamani, Hydrothermal fabrication and characterization of novel $CeO_2/PbWO_4$ nanocomposite for enhanced visible-light photocatalytic performance, Appl. Water Sci. 11 (2021) 93. DOI: https://doi.org/10.1007/s13201-021-01429-x

[25] Y. Wang, H. Wang, X. Wang, J. Zhang, G. Wang, X. Zhang, Facile synthesis of S-scheme Bi_2S_3/BiOCl heterojunction with tunable bandgap structures for enhanced photocatalytic organic degradation performance, Inorg. Chem. Commun. 171 (2024) 113532. DOI: https://doi.org/10.1016/j.inoche.2024.113532

[26] Z.H. Jabbar, B.H. Graimed, A.A. Okab, H.S. Merdas, A.M. El-Sulaiman, A. Majdi, Economic photocatalytic degradation of environmental pollutants over $CuBi_2O_4/Ag_2CrO_4$ photocatalyst with core-shell heterostructure: S-scheme mechanism, J. Cluster Sci. 36 (2025) 89. DOI: https://doi.org/10.1007/s10876-025-02803-4

[27] C. Chen, J. Zhang, H. Chu, L. Sun, G. Dawson, K.Dai, Chalcogenide-based S-scheme heterojunction photocatalysts, Chinese J. Catal. 63 (2024) 81–108. DOI: https://doi.org/10.1016/S1872-2067(24)60072-0

[28] B. Parasuraman, P. Shanmugam, P. Govindasamy, S. Nangan, L. Gnanasekaran, P. Thangavelu, Photocatalytic degradation of tetracycline contaminated wastewater over $Bi_2S_3/BiWO_6$/rGO ternary nanocomposite under visible light irradiation, J. Taiwan Inst. Chem. Eng. 166 (2025) 105249. https://doi.org/10.1016/j.jtice.2023.105249

[29] Y.-D. Sun, C. Zeng, X. Zhang, Z.-Q. Zhang, B. Yang, S.-Q. Guo, Tendencies of alloyed engineering in BiOX-based photocatalysts: a state-of-the-art review, Rare Metal. 43 (2024) 1488–1512. DOI: https://doi.org/10.1007/s12598-023-02569-6

[30] J. Liu, J. Shi, H. Deng, Current status of research on BiOX-based heterojunction photocatalytic systems: Synthesis methods, photocatalytic applications and prospects, J. Environ. Chem. Eng. 11 (2023) 110311. DOI: https://doi.org/10.1016/j.jece.2023.110311

[31] L. Chen, B. Guan, J. Guo, Y. Chen, Z. Ma, J. Chen, S. Yao, C. Zhu, H. Dang, K. Shu, Review on the preparation and performance improvement methods of bismuth photocatalyst materials, Catal. Sci. Technol. 13 (2023) 5478–5529. DOI: https://doi.org/10.1039/D3CY00760J

[32] D.O. Alshahrani, M.A. Nadeem, A. Mujtaba, M. Khan, L.B. Farhat, A. Nasir, U. Younas, Tailoring the tungsten sulfide nanoparticles by nickel doping for high-performance energy storage application, J. Indian Chem. Soc. 102 (2025) 101709. DOI: https://doi.org/10.1016/j.jics.2025.101709

[33] L. Peng, R. Zhang, Q. Lei, J. Luo, A comparison study of the photocatalytic mechanism and performance of Bi_2S_3-based binary composite (Cu_2O/Bi_2S_3) and ternary composite (NH_2-UiO-66/BiOBr/Bi_2S_3) photocatalyst for tetracycline degradation under visible-light irradiation, Int. J. Environ. Anal. Chem. 103 (2023) 7476–7493. DOI: https://doi.org/10.1080/03067319.2021.1972100

[34] A. Nazir, M.S. Tahir, G.M. Kamal, X. Zhang, M.B. Tahir, B. Jiang, M. Safdar, Fabrication of ternary $MoS_2/CdS/Bi_2S_3$-based nano composites for photocatalytic dye degradation, Molecules 28 (2023) 3167. DOI: https://doi.org/10.3390/molecules28073167

[35] X. Chen, W. Zhang, L. Zhang, L. Feng, J. Wen, J. Yang, C. Zhang, J. Jiang, H. Wang, Effective photocatalytic salicylic acid removal under visible light irradiation using

Ag_2S/AgI-Bi_2S_3/BiOI with Z-scheme heterojunctions, Appl. Surf. Sci. 481 (2019) 1335–1343. DOI: https://doi.org/10.1016/j.apsusc.2019.03.214

[36] L. Kan, W. Mu, C. Chang, F. Lian, Dual S-scheme graphitic carbon-doped α-Bi_2O_3/β-Bi_2O_3/Bi_5O_7I ternary heterojunction photocatalyst for the degradation of Bisphenol A, Separat. Purif. Technol. 312 (2023) 123388. DOI: https://doi.org/10.1016/j.seppur.2023.123388

[37] A. Etogo, E. Hu, C. Zhou, Y. Zhong, Y. Hu, Z. Hong, Facile fabrication of mesoporous BiOCl/$(BiO)_2CO_3$/Bi_2O_3 ternary flower-like heterostructured microspheres with high visible-light-driven photoactivity, J. Mater. Chem. A, 3 (2015) 22413–22420. DOI: https://doi.org/10.1039/C5TA06082F

[38] H.P. del Pulgar, J. Ortiz-Bustos, A. Torres-Pardo, M. Parras, I. del Hierro, Y. Pérez, Innovative ternary composite photocatalyst: BiOCl/$Bi_{12}O_{17}Cl_2$/Bi_2O_3 for sustainable water remediation, Appl. Surf. Sci. 660 (2024) 160028. DOI: https://doi.org/10.1016/j.apsusc.2024.160028

[39] Y. Peng, P.-P. Yu, H.-Y. Zhou, A.-W. Xu, Synthesis of BiOI/$Bi_4O_5I_2$/$Bi_2O_2CO_3$ p–n–p heterojunctions with superior photocatalytic activities, New J. Chem. 39 (2015) 8321–8328. DOI: https://doi.org/10.1039/C5NJ01662B

[40] M.A. Sayed, S.M.A. El-Gamal, M. Ramadan, F.M. Helmy, A. Mohsen, Hydrothermal synthesis and structural optimization of Bi_2O_3/Bi_2WO_6 nanocomposites for synergistic photodegradation of Indigo Carmine dye, Sci. Rep. 15 (2025) 17260. DOI: https://doi.org/10.1038/s41598-025-01925-z

[41] S. Surendhiran, K. Balu, A. Karthik, V. Rajendran, Biogenic synthesis of CeO_2 nanoparticles via moringa oleifera seed extract: Photocatalytic and biological activity for

textile dye degradation, J. Indian Chem. Soc. 101 (2024) 101302. DOI: https://doi.org/10.1016/j.jics.2024.101302

[42] Y. Qin, Y. Zhang, J. Wang, J. Zhang, Y. Zhai, H. Wang, D. Li, Heterogeneous structured Bi_2S_3/MoS_2@NC nanoclusters: exploring the superior rate performance in sodium/potassium ion batteries, ACS Appl. Mater. Interf. 12 (2020) 42902–42910. DOI: https://doi.org/10.1021/acsami.0c13070

[43] A. Somdee, S. Wannapop, N. Pijarn, T. Bovornratanaraks, Enhanced charge carrier density of a p-n BiOCl/$BiVO_4$ heterostructure by Ni doping for photoelectrochemical applications, J. Alloy. Comp. 937 (2023) 168434. DOI: https://doi.org/10.1016/j.jallcom.2022.168434

[44] J.-C. Wang, H. Ma, W. Shi, W. Li, Z. Zhang, Y. Hou, W. Zhang, J. Chen, Designed synthesized step-scheme heterojunction of Bi_2WO_6 nanosheet supported on $CuBi_2O_4$ nanorod with remarkable photo-assisted gas sensing for N-butyl alcohol, J. Environ. Chem. Eng. 12 (2024) 112698. DOI: https://doi.org/10.1016/j.jece.2024.112698

[45] X. Yao, X. Jiang, D. Zhang, S. Lu, M. Wang, S. Pan, X. Pu, J. Liu, P. Cai, Achieving improved full-spectrum responsive 0D/3D $CuWO_4$/BiOBr: Yb^{3+}, Er^{3+} photocatalyst with synergetic effects of up-conversion, photothermal effect and direct Z-scheme heterojunction, J. Colloid Interf. Sci. 644 (2023) 95–106. DOI: https://doi.org/10.1016/j.jcis.2023.04.072

[46] J.C. Durán-Álvarez, B. Vargas, D. Mejía, S. Cortés-Lagunes, A. Serrano-Lázaro, O. Ovalle-Encinia, R. Zanella, C.A. Rodríguez, Synthesis of highly crystalline BiOI thin films for the photocatalytic removal of antibiotics in tap water and secondary effluents:

Assessing the potential hazard of treated water, J. Environ. Chem. Eng. 12 (2024) 114590. DOI: https://doi.org/10.1016/j.jece.2024.114590

[47] M. Sattari, M. Farhadian, A. Reza Solaimany Nazar, M. Moghadam, Enhancement of Phenol degradation, using of novel Z-scheme $Bi_2WO_6/C_3N_4/TiO_2$ composite: Catalyst and operational parameters optimization, J. Photochem. Photobiol. A: Chem. 431 (2022) 114065. DOI: https://doi.org/10.1016/j.jphotochem.2022.114065

[48] P.-M.A.K. Sone, C.B.D. Nguela, C.G. Fotsop, A.V. Abega, A.K. Tamo, D. Kouotou, N.J. Nsami, Innovative ternary bismuth oxychloride/bismuth oxide/carbon nanotubes induced excellent solar light-driven activity toward photomineralisation of diclofenac: Impact of metastable β-Bi_2O_3 inserted and electron-hole separation, Result. Chem. 7 (2024) 101497. DOI: https://doi.org/10.1016/j.rechem.2024.101497

[49] T.I. Alanazi, Boosting the structural, electrical properties, and optical features of porous starch/poly (ethylene oxide) reinforced with $NiMoO_4$ nanocrystals, J. Mater. Sci.: Mater. Electron. 36 (2025) 16. DOI: https://doi.org/10.1007/s10854-024-14077-z

[50] M.A. Qamar, M. Javed, S. Shahid, S. Iqbal, S.A. Abubshait, H.A. Abubshait, S.M. Ramay, A. Mahmood, H.M. Ghaithan, Designing of highly active g-C_3N_4/Co@ ZnO ternary nanocomposites for the disinfection of pathogens and degradation of the organic pollutants from wastewater under visible light, J. Environ. Chem. Eng. 9 (2021) 105534. DOI: https://doi.org/10.1016/j.jece.2021.105534

[51] A. Dolgonos, T.O. Mason, K.R. Poeppelmeier, Direct optical band gap measurement in polycrystalline semiconductors: A critical look at the Tauc method, J. Solid State Chem. 240 (2016) 43–48. DOI: https://doi.org/10.1016/j.jssc.2016.05.010

[52] H. Li, Y. Cui, W. Hong, High photocatalytic performance of BiOI/Bi_2WO_6 toward toluene and Reactive Brilliant Red, Appl. Surf. Sci. 264 (2013) 581–588. DOI: https://doi.org/10.1016/j.apsusc.2012.10.068

[53] Y. Wei, C. Liu, X. Li, H.-Y. Wang, Y.-M. Yang, G.-F. Shi, G.-Y. Wang, Construction of S-scheme BiOCl/$Bi_{24}O_{31}Cl_{10}$ heterojunction by thermally induced in-situ phase transition strategy for photocatalytic degradation of ciprofloxacin, J. Water Process Eng. 69 (2025) 106795. DOI: https://doi.org/10.1016/j.jwpe.2024.106795

[54] B. Zhu, G. Jiang, S. Chen, F. Liu, Y. Wang, C. Zhao, Multifunctional Cl-S double-doped carbon nitride nanotube unit in catalytic ozone oxidation synergistic photocatalytic system: Generation of ROS-rich region and effective treatment of organic wastewater, Chem. Eng. J. 430 (2022) 132843. DOI: https://doi.org/10.1016/j.cej.2021.132843

[55] S. Li, T. Huang, P. Du, W. Liu, J. Hu, Photocatalytic transformation fate and toxicity of ciprofloxacin related to dissociation species: Experimental and theoretical evidences, Water Res. 185 (2020) 116286. DOI: https://doi.org/10.1016/j.watres.2020.116286

[56] M.E. dos Santos Soldan, E.B. Lied, I.L.C. Junior, P.R.S. Bittencourt, I.J. Baraldi, R.M. Giona, A.P. Trevisan, F.H. Passig, K.Q. de Carvalho, Optimizing ciprofloxacin removal using ion exchange resin: exploring operational parameters and assessing toxicity, Chem. Eng. Sci. 282 (2023) 119317. DOI: https://doi.org/10.1016/j.ces.2023.119317

[57] F. Azeez, E. Al-Hetlani, M. Arafa, Y. Abdelmonem, A.A. Nazeer, M.O. Amin, M. Madkour, The effect of surface charge on photocatalytic degradation of methylene blue dye using chargeable titania nanoparticles, Sci. Rep. 8 (2018) 7104. DOI: https://doi.org/10.1038/s41598-018-25673-5

[58] M. Sher, M. Javed, S. Shahid, S. Iqbal, M.A. Qamar, A. Bahadur, M.A. Qayyum, The controlled synthesis of gC_3N_4/Cd-doped ZnO nanocomposites as potential photocatalysts for the disinfection and degradation of organic pollutants under visible light irradiation, RSC Adv. 11 (2021) 2025–2039. DOI: https://doi.org/10.1039/D0RA08573A

[59] A. Amari, H.S. Sultan Aljibori, N. Elboughdiri, Z. Algarni, M.A. Ismail, A.A.H. Kadhum, I. Mahariq, Synthesis of a highly efficient ternary Heterostructure for synergistic charge migration: Dual-functional enhancement in photocatalytic ciprofloxacin degradation and hydrogen production, J. Water Process Eng. 65 (2024) 105841. DOI: https://doi.org/10.1016/j.jwpe.2024.105841

[60] Z. Li, D. Lan, Z. Li, J. Sun, S. Chen, J. Yang, J. Wei, Z. Yu, S. Wang, Y. Hou, Step-doped disulfide vacancies and functional groups synergistically enhance photocatalytic activity of S-scheme Cu_3SnS_4/L-BiOBr towards ciprofloxacin degradation, Chemosphere 301 (2022) 134684.

[61] J. Niu, K. Wang, L. Yang, J. Shi, Y. Zhang, F. Yang, X. Yu, B. Yao, Construction of a novel g-C_3N_4@Bi/BiOBr ternary heterojunction with Z-scheme mechanism for the efficient photocatalytic removal of ciprofloxacin, Optic. Mater. 134 (2022) 113125. DOI: https://doi.org/10.1016/j.optmat.2022.113125

[62] X. Liu, Z. Cheng, L. Lin, W. Xu, S. Chen, H. Zhuang, Fabrication of ternary Bi_2S_3/$BiVO_4$/g-C_3N_4 composite material for enhanced photocatalytic degradation of antibiotics, Diamond Relat. Mater. 148 (2024) 111376. DOI: https://doi.org/10.1016/j.diamond.2024.111376

[63] Y. Jin, Z. Xing, Y. Li, J. Han, H. Lorenz, J. Chen, Synthetic BiOBr/Bi_2S_3/CdS crystalline material and its degradation of dye under visible light, Crystals 11 (2021) 899. DOI: https://doi.org/10.3390/cryst11080899

[64] M. Naeem, M. Imran, S. Latif, BiOX/Bi_2MoO_6 /Bi_2O_3 (X = Cl, Br, I) ternary composites forefficient degradation of ciprofloxacin from wastewater driven by visible light, ChemistrySelect 10 (2025) e04390. DOI: https://doi.org/10.1002/slct.202504390

[65] X. Zeng, Y. Zhou, W. He, M. Dang, Y. Zhou, G. Huang, D. Feng, J. Zhang, Efficient photocatalytic degradation of ciprofloxacin by doped $Bi_4O_5I_2$ with Gd^{3+} as an electron trap: Gd^{3+} substitutes Bi^{3+} in the lattice, J. Phys. Chem. Solid. 188 (2024) 111891. DOI: https://doi.org/10.1016/j.jpcs.2024.111891

Declaration of interests

☒ The authors declare that they have no known competing financial interests or personal relationships that could have appeared to influence the work reported in this paper.

☐ The authors declare the following financial interests/personal relationships which may be considered as potential competing interests:

Graphical Abstract

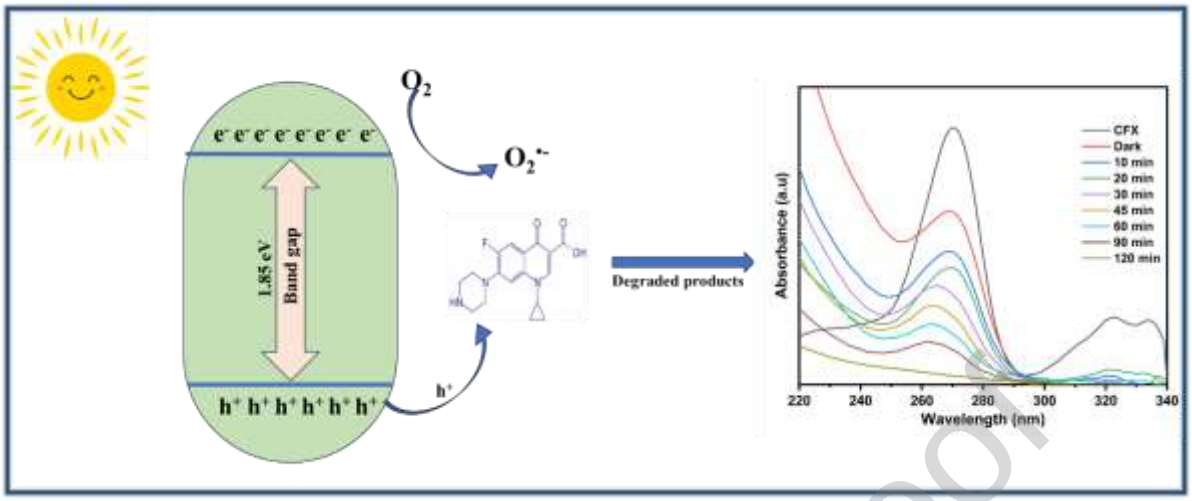

Highlights

- Synthesized BiOX/Bi_2WO_6/Bi_2S_3 heterostructures for visible-light photocatalysis
- The heterojunctions showed excellent visible-light photodegradation of CFX
- The ternary BiOX/Bi_2WO_6/Bi_2S_3 heterojunctions showed stability and reusability
- The synthesized heterojunctions showed enhanced charge separation
- Holes and superoxide radicals played dominant roles in photodegradation